Challenges and opportunities for photonic sensing of key atmospheric short-lived species

***W. Chen*[1], R. Maamary[1], X. Cui[1,2], T. Wu[1,3], E. Fertein[1], C. Coeur[1], A. Cassez[1], W. Liu[2], F. Dong[2], Y. Wang[2], W. Zhang[2], X. Gao[2], G. Zha[4], Z. Xu[4], T. Wang[4]**

[1]Laboratory of Physical Chemistry of the Atmosphere, University of the Littoral Opal Coast, France

[2]Anhui Institute of Optics & Fine Mechanics, Chinese Academy of Sciences, Hefei, China

[3]Key Laboratory of Nondestructive Test, Nanchang Hang Kong University, Nanchang, China

[4]Department of Civil and Structural Engineering, The Hong Kong Polytechnic University, Hong Kong


Manchester
Rotherham
Leicester
Norwich
Amsterdam
Zwolle
Birmingham
Ipswich
Den Haag
Nederland
Swansea
London
Netherlands
Bristol
Cardiff
Dunkerque
Belgie
Venlo
Belgique
Brighton
Southampton
Lille
Belgium
Plymouth
Le Havre
Amiens
Luxembourg
Reims
Rouen
Paris
Caen
Metz
Nancy
Brest
Rennes
Le Mans
Strasbourg
Quimper
Orléans
Nantes
Tours
Bourges
Dijon
Besançon
Cholet
Poitiers
France
Lausanne
La Rochelle
Niort
Limoges
Lyon
Genève
Saint-Etienne
Bordeaux
Grenoble
Torino

Dunkerque campus

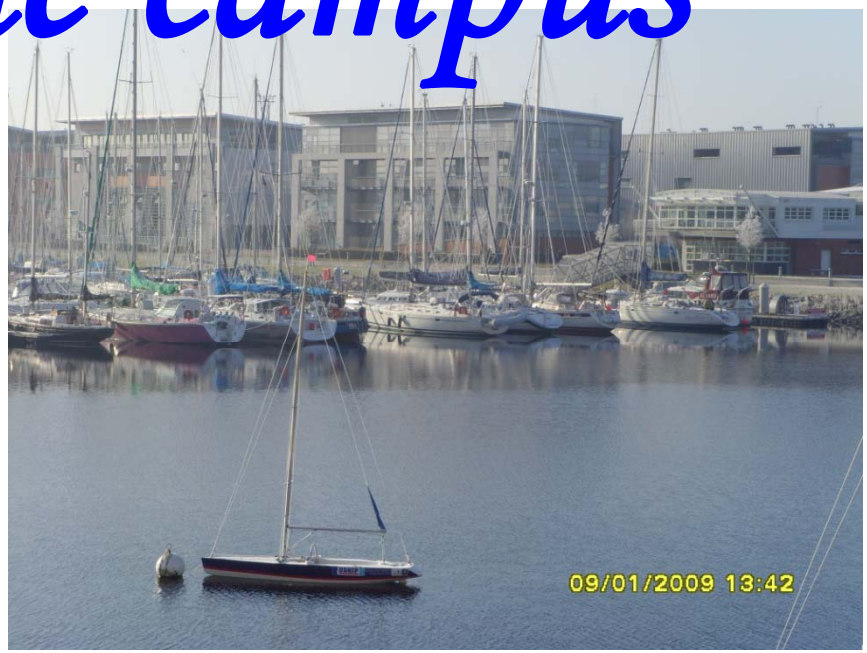

Outline of Talk

- **Introduction**
  - Motivation & Challenge
  - State of the art spectroscopic technologies
  - Spectral manipulation
- **Photonic sensing by IR lasers**
  ICOS – FSR – Multipass direct absorption
- **Photonic sensing by UV-VIS LEDs**
  IBBCEAS
- **Applications**
  - Field observation
  - Chemical reaction study in smog chamber
- **Summary**

Motivation

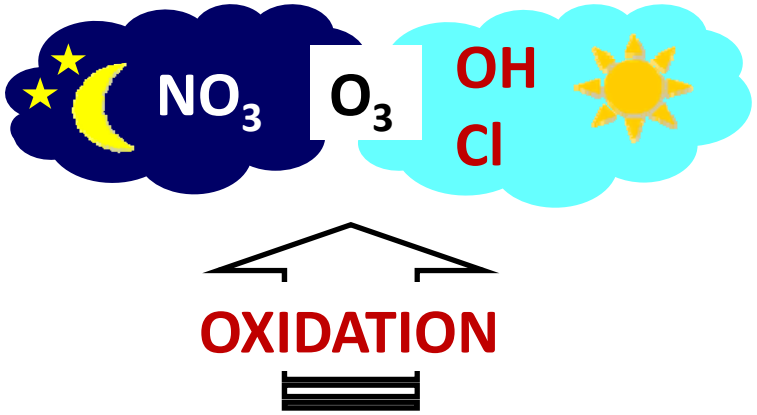

GHG, VOCs, BVOCs, HCs, NOx, DMS, …

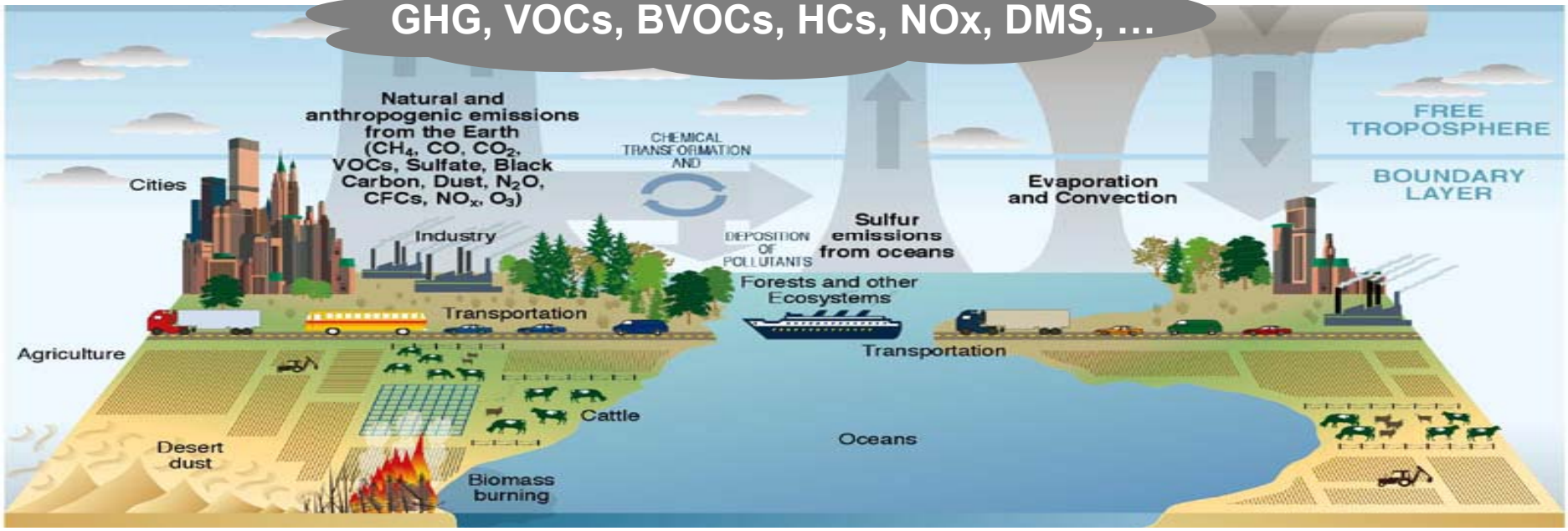

Motivation

(Prinn 2003)

Trace gas	Global emission rate (Tg/yr)	Removal by OH (%)
CO	2800	85
CH_4	530	90
C_2H_6	20	90
Isoprene	570	90
Terpenes	140	50
NO_2	150	50
SO_2	300	30
$(CH_3)_2S$	30	90

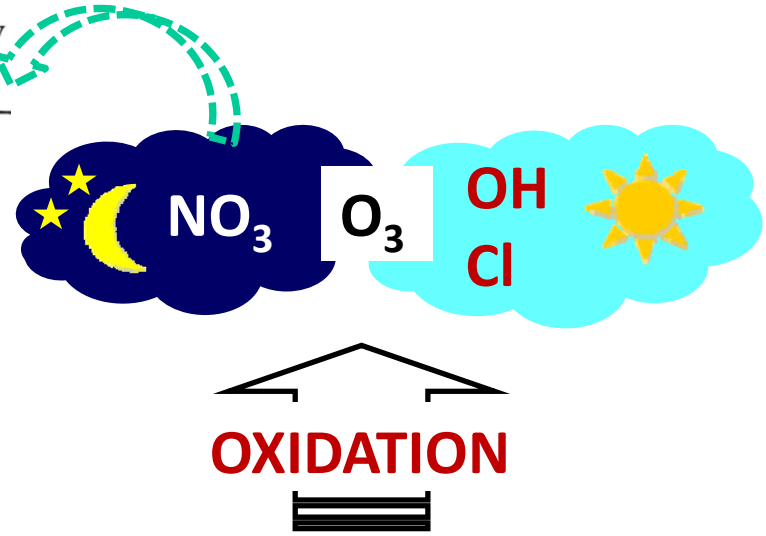

GHG, VOCs, BVOCs, HCs, NOx, DMS, …

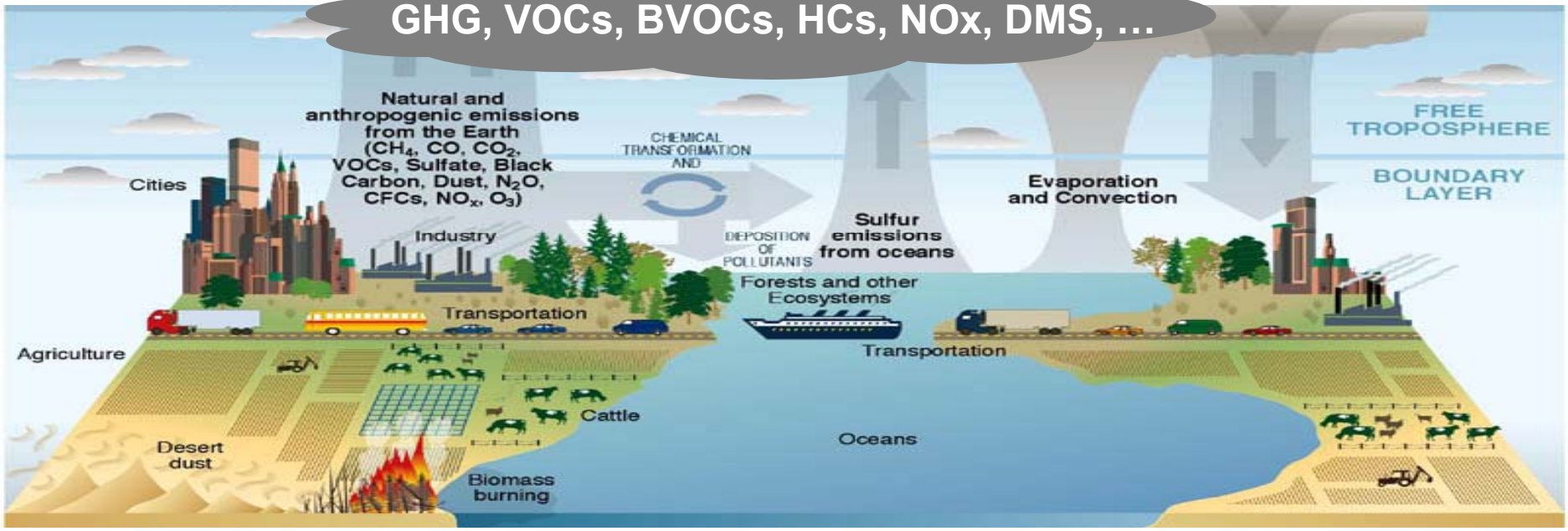

Motivation

[OH] ~ 10^6 cm^{-3} (0.1 pptv)

[O_3] ~ 10^{11} cm^{-3} (10 ppbv)

[NO_3] ~ 10^8 cm^{-3} (10 pptv)

[Cl] = 10^3-10^5 cm^{-3} (0.1-10 ppqv)

NO_3 production

$NO_2 \xrightarrow{O_3} NO_3$

$N_2O5 \rightleftharpoons NO_3 + NO_2$

OH production

$HONO \xrightarrow{h\nu} OH$

$O_3 \xrightarrow{h\nu, H_2O} OH$

$HCHO \xrightarrow{h\nu, O_2} HO_2 \xrightarrow{NO} OH$

$RO_2 \xrightarrow{NO} HO_2 \xrightarrow{NO} OH$

O_3 production

$O(^3P) + O_2 \rightarrow O_3$

$O_3 \xrightarrow[\lambda < 850\ nm]{h\nu} O(^3P) + O_2$

$NO_2 \xrightarrow[\lambda < 420\ nm]{h\nu} O(^3P) + NO$

GHG, VOCs, BVOCs, HCs, NOx, DMS, …

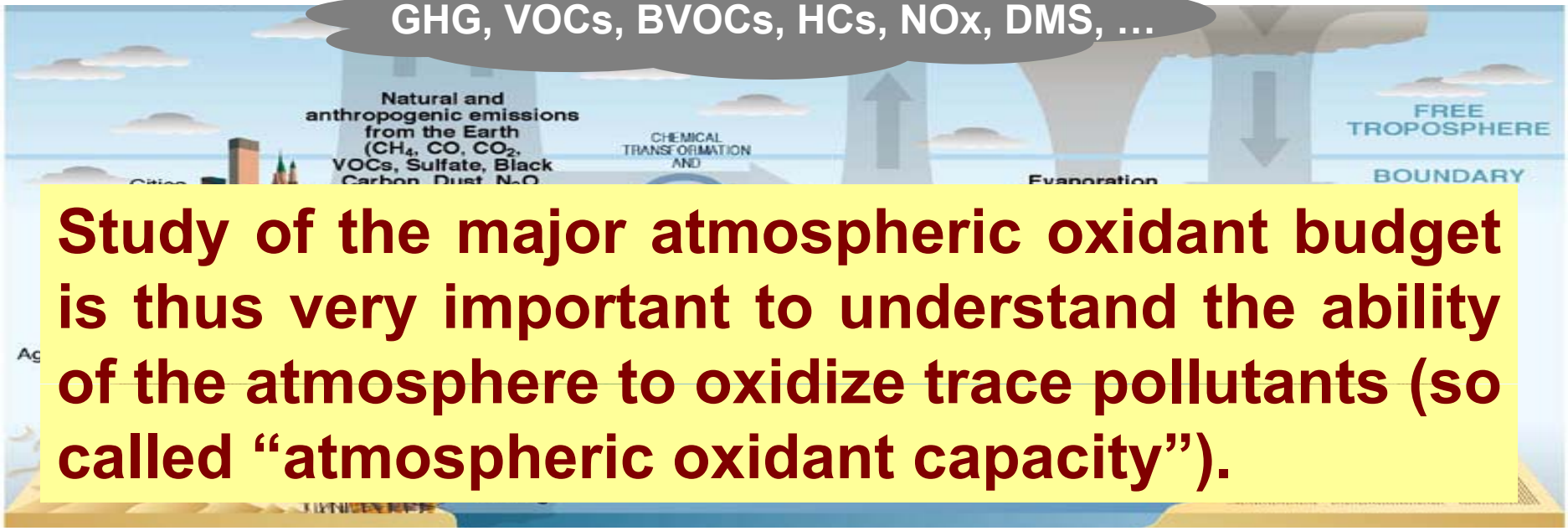

Study of the major atmospheric oxidant budget is thus very important to understand the ability of the atmosphere to oxidize trace pollutants (so called "atmospheric oxidant capacity").

Motivation

[OH] ~ 10^6 cm^{-3} (0.1 pptv)

[O_3] ~ 10^{11} cm^{-3} (10 ppbv)

[NO_3] ~ 10^8 cm^{-3} (10 pptv)

[Cl] = 10^3-10^5 cm^{-3} (0.1-10 ppqv)

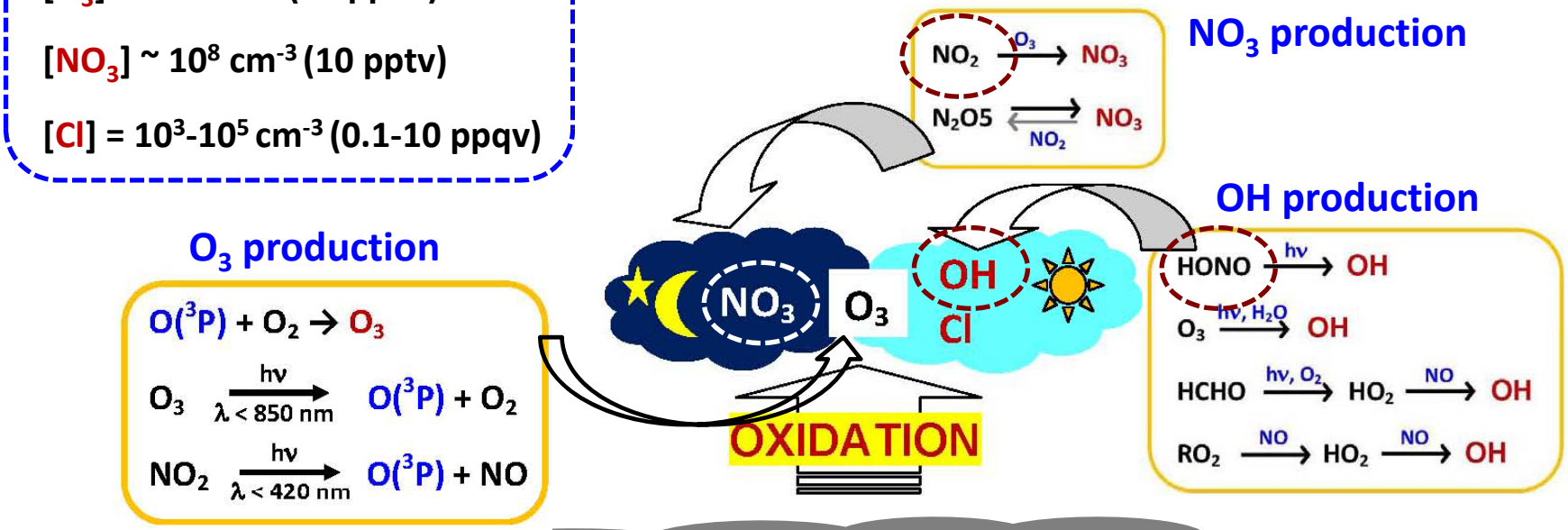

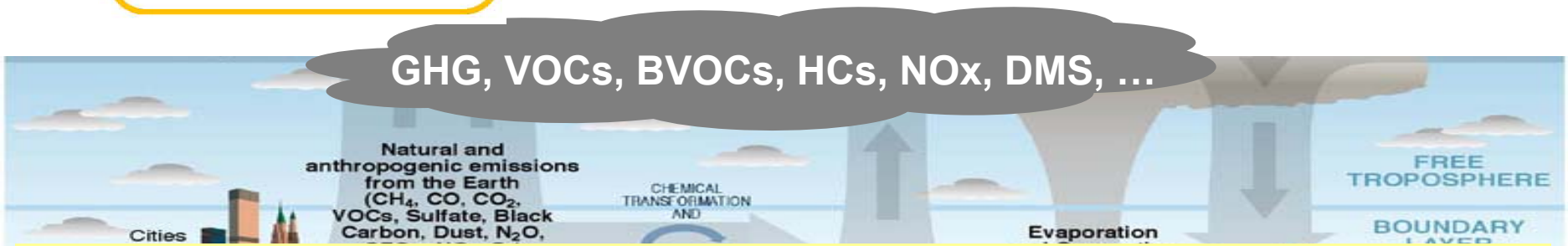

Precise concentration assessment of the key atmospheric oxidants and their precursors is very important for understanding & prediction of regional air quality and global climate change.

Challenges

No commercially available instruments for direct concentration measurements. All routine measurements are based on ***chemical conversion + measurements with IC, FL, CL, LOPAP, HPLC***.

Main problem : ***chemical interference*** due **to sample preparation** (such as *species separation, trapping, chemical conversion, ionization, pre-concentration*, etc.) and ***analytical artifacts***

Photonic sensing => non-intrusive measurements with ***fast time response, high specificity without additional sample preparation***

Challenges

- Ultralow concentration : ppb (10^{-9}) - ppq (10^{-15});
- Very short lifetime : down to seconds;
- Free of chemical interference;
- No standard gas reference available for validation and calibration;
- No spectral data available in the common databases (HITRAN, ..)

High performance probing source-detector & sensitive sensing scheme

+

Lab. production of sample & Intercomparison campaigns

CW mid-Infrared Lasers (fdt ro-vibration)

DFB Quantum Cascade Lasers (QCL) : 4 - 16 µm

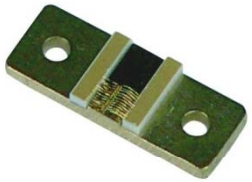

~ 20 k$

CW output power : 10 mW to > 1 W (@ TEC)

Limited spectral coverage : < 10 cm^{-1}

Interband Cascade Lasers (ICL) : 3 - 6 µm

External cavity QCL : 4.4 - 10.5 µm

~ 50 k$

CW output power : > 70 mW

Wide spectral coverage : > 30 cm^{-1} up to ~ 400 cm^{-1}

Quantum well DFB lasers : 2.9 – 3.5 µm

< 10 k$

CW output power : > 1 mW

Limited spectral coverage : < 10 cm^{-1}

Multi-chip laser sources : 6-13 µm / 3 chips
in pulsed operation

→ **CW mode?**

Optical parametrical sources: DFG, OPO (powerful tool for lab. study

Broadband light sources

Sources	Xenon arc lamp 	Light Emitting Diode (LED)  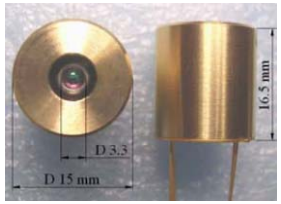		Superconituum (white light) 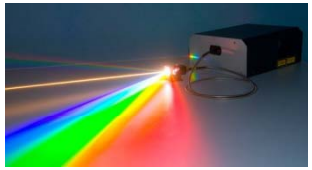
Spectral Range	185 – 2000 nm	350 – 1550 nm	3 – 7 µm	400 – 2200 nm
Linewidth (FWHM)	180 – 2000 nm	~ 20 nm (UV) > 100 nm (VIS)	0.4 – 2 µm (0.1 - 0.2 λ_{max})	400 – 2200 nm
Beam Quality	Black body emission in all direction*	Vieing half angle $\theta_{1/2} = \pm$ (7-70) °	≤ 40 °	laser-like beam quality (ϕ2 mm @ 633 nm)
Optical Power Output	35 – 300 W	50 - 1000 mW	10 – 500 µW	6 W
Cooling	Convection cooling	TE cooling	TE cooling	air-cooling
Cost	~ 5000 € (system) **	10 – 60 $	~ 100 $	Some tens of k$

* $\theta_{1/2}$=0.8°& ϕ33 mm after collimation; ** ~ 150 € per lamp (75 W)

High sensitivity spectroscopy techniques

(high sensitivity => high Signal to Noise Ratio, SNR)

✓ **Long optical path length absorption spectroscopy ("S"↗)**

- **Multipass cell => 100-200 m (ppm-ppb)**
- **Optical cavity (Cavity enhanced spectroscopy :**

OA-ICOS, IBBCEAS, CRDS) => 1-10 km (ppb-ppt)

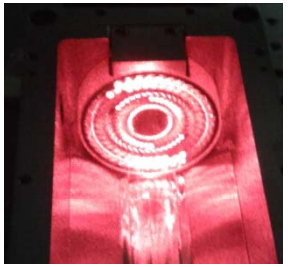

✓ **Low noise spectroscopic detection approaches ("N"↘)**

1) Light modulation-phase sensitive detection methods:

- **Frequency / Wavelength Modulation Spectroscopy (FMS / WMS) => BG free**

2) Indirect measurements (of absorption induced physical parameter from which the absorber concentration can be inferred)

- **CRDS => BG free**
- **Photoacoustic spectroscopy (PAS / QEPAS) => BG free**
- **Faraday rotation spectroscopy (FRS) => BG free**

Spectral manipulation : Lineshape fits using Voigt and Galatry profiles for integrated area determination

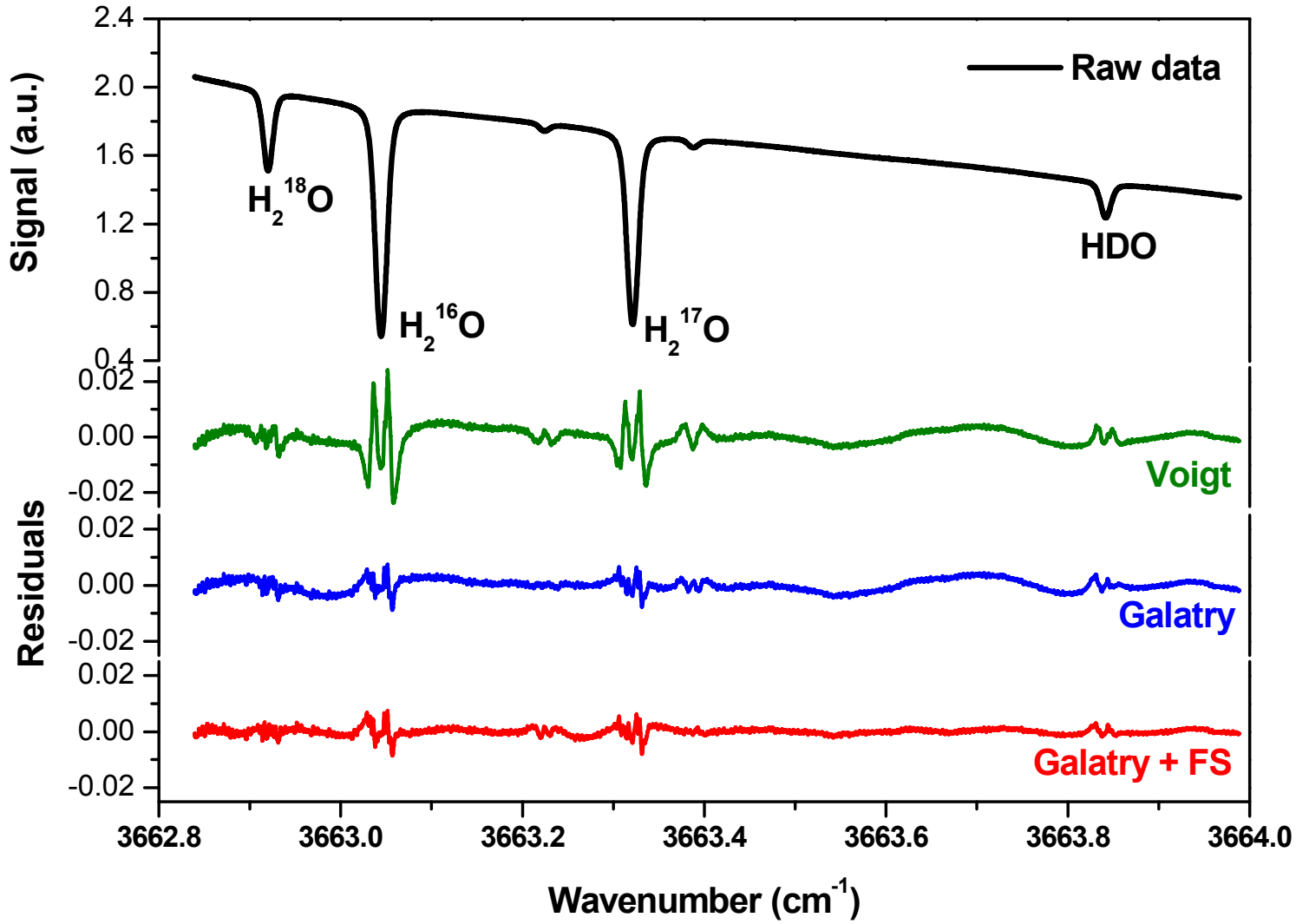

Spectral manipulation : « Fourier filtering »

for cancellation of the oscillation structure in baseline

Fourier transform of residual spectrum

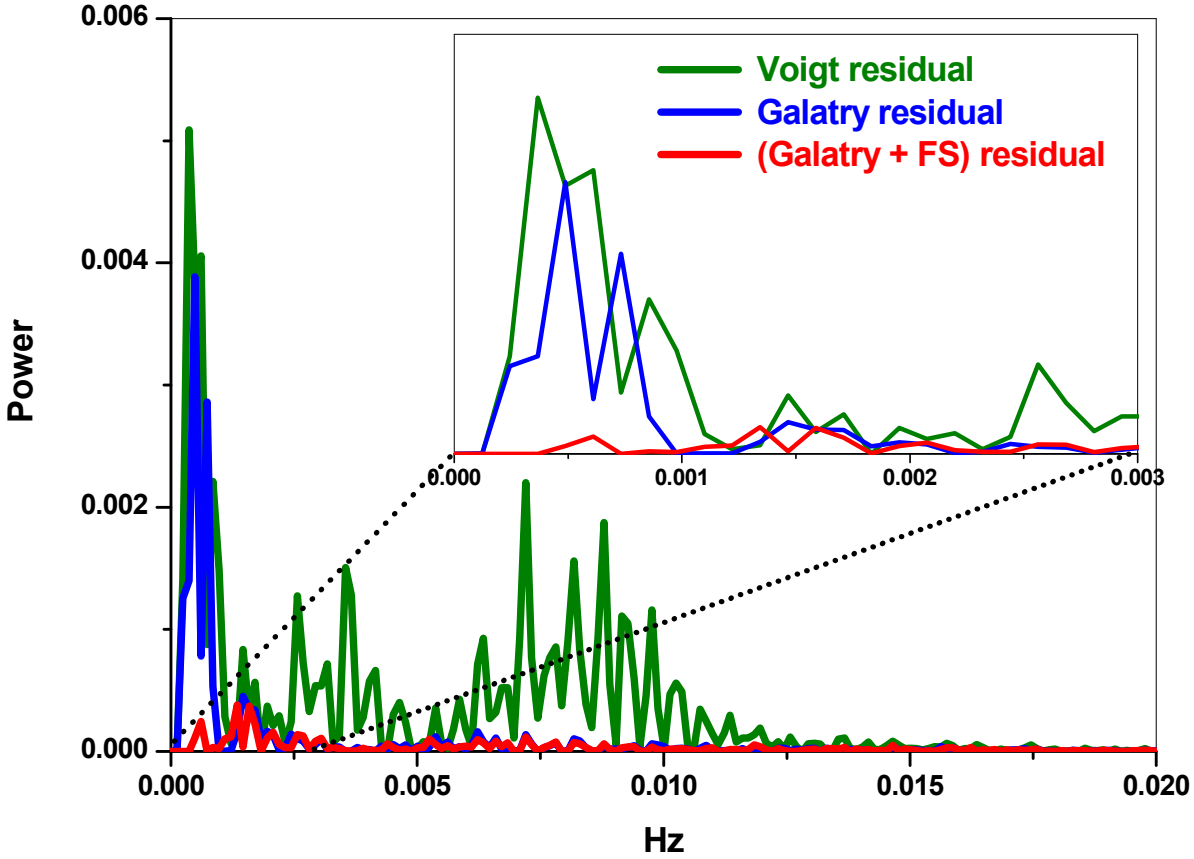

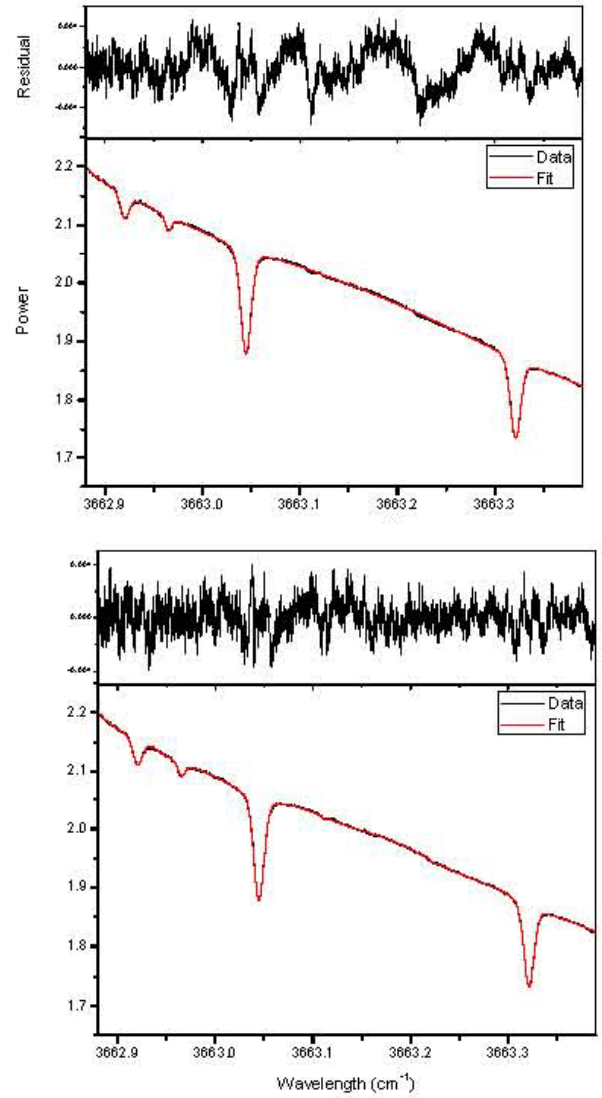

Spectral manipulation : Improvement in measurement precision

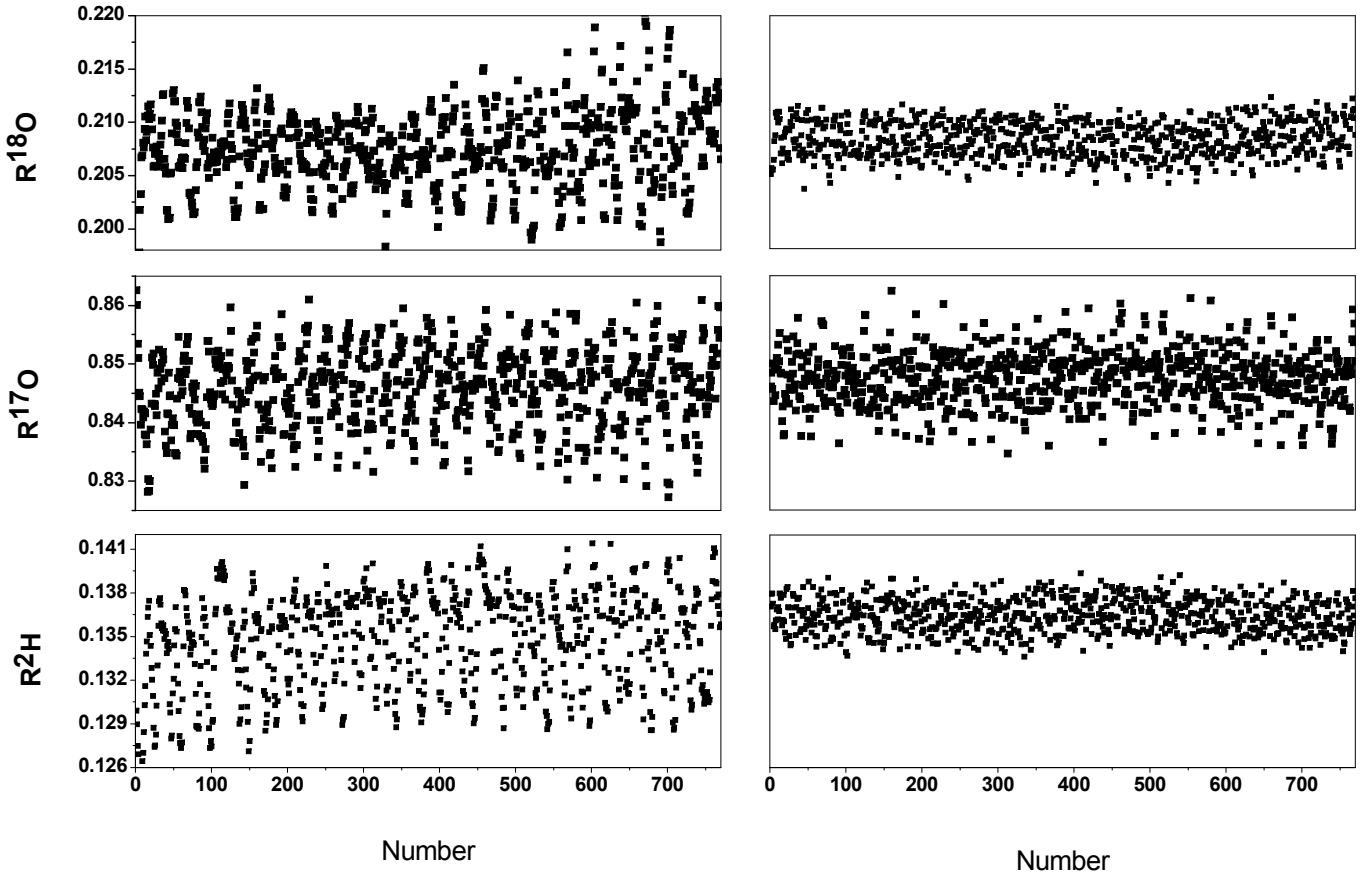

Left panel : Before (left panel) and after (right panel) spectral manipulation

➢ **up to 3-fold reduction in standard deviation**

Spectral manipulation : « Kalman filtering »

Kalman filtering, originally developed by R.E. Kalman for aerospace navigation applications (*J. Basic Eng.* ***82*** *(1960) 35*), uses a recursive procedure for "true value" prediction based on the previously determined value : **filtering out the shot-to-shot real-time noise while following the true variation in measured physical quantity.**

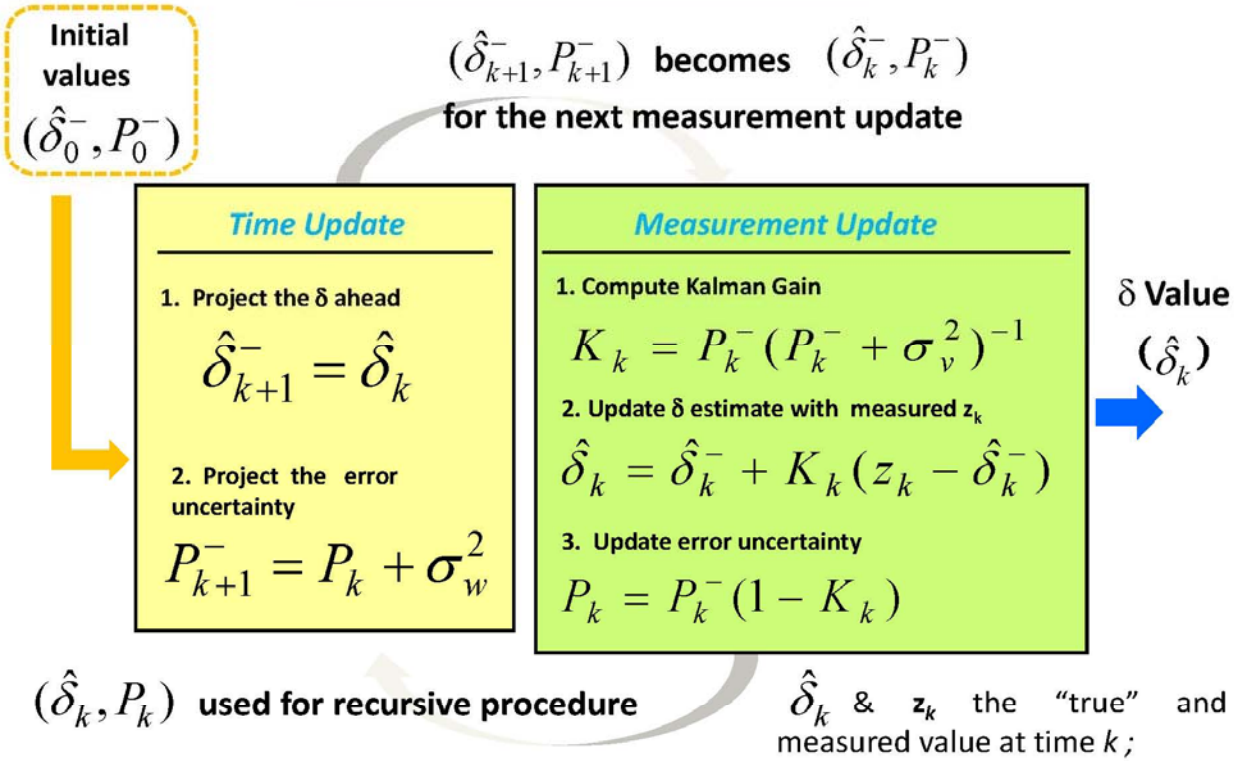

$\hat{\delta}_k$ & z_k the "true" and measured value at time *k* ;

σ_v^2, σ_w^2 the measurement noise and process variability.

D.P. Leleux, R. Claps, W. Chen, F.K. Tittel, T.L. Harman, Appl. Phys. B**74**, 85 (2002)

Time series of the δ-value for ^{18}O, ^{17}O and ^{2}H in water

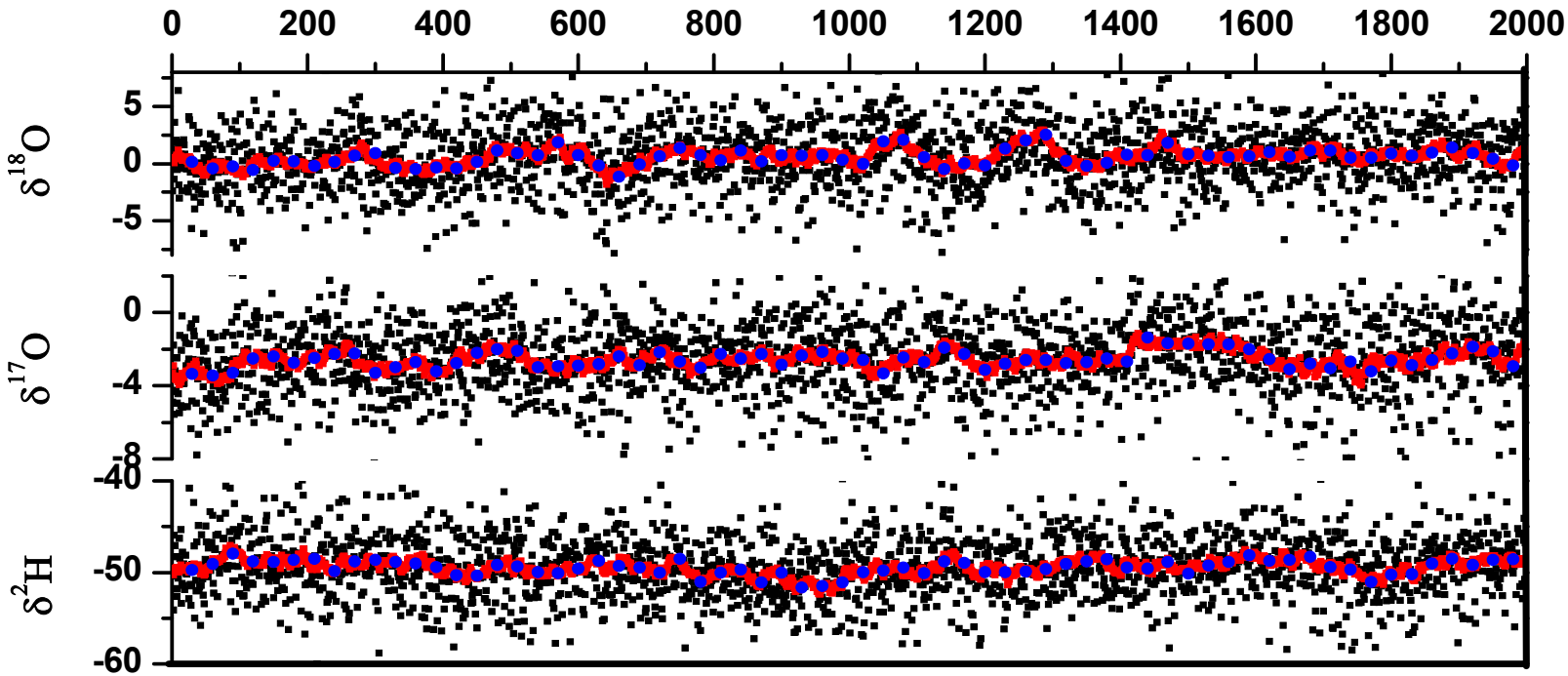

Raw measurement of the δ-value for ^{18}O, ^{17}O, ^{2}H (black dots, in 1-s), the corresponding Kalman filter output (red lines, q=150 in 1-s), and the averaged value of 30 δ values (blue dots, in 30-s).

Kalman filtering : high measurement precision while keeping a fast system response, not affecting the mean value of the data.

Ref. T. Wu, W. Chen et al, Opt. Lett. **35** (2010) 634-636

Photonic sensing by IR lasers

ICOS – FSR – Multipass cell

OH radical concentration measurements

Lifetimes : ~ 1 s in clean air

< 1 s in polluted environment

Typical concentration : 10^5 – 10^7 OH/cm^3 or 0.01-1 ppt @ STP

- ✓ primary "cleansing agent" removing pollutants in the atmosphere
- ✓ initiating reactions leading to the production of O_3
- ✓ effecting on the formation of aerosol

Current OH sensing technologies

Spectroscopic methods currently used for measurements of OH :

- Long-path Differential Optical Absorption Spectroscopy (DOAS)
- Laser induced Fluorescence Assay by Gas Expansion (FAGE)

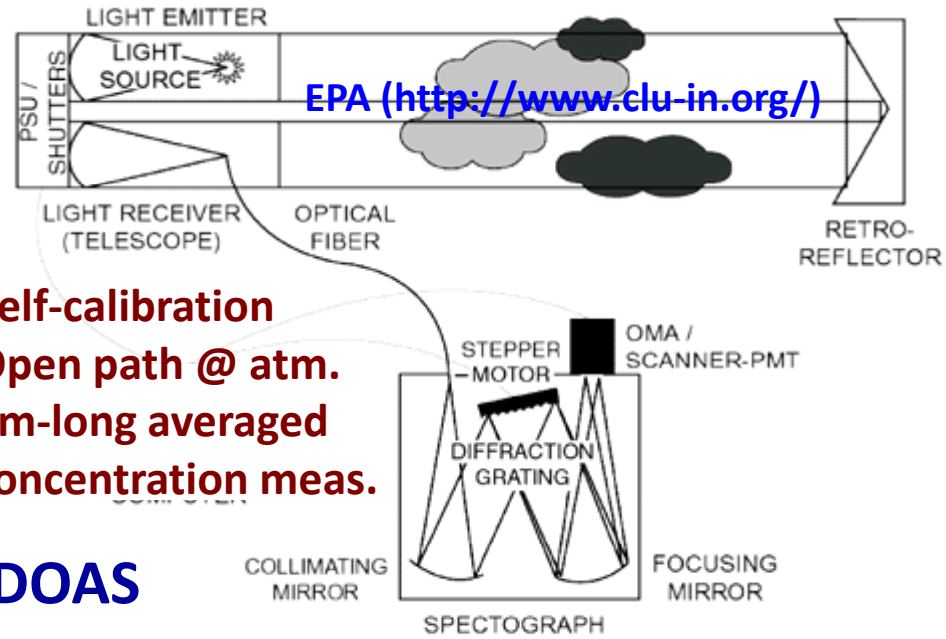

* Self-calibration
* Open path @ atm.
* km-long averaged concentration meas.

DOAS

*sensitive to visibility conditions
*low spectral & spatial resolution

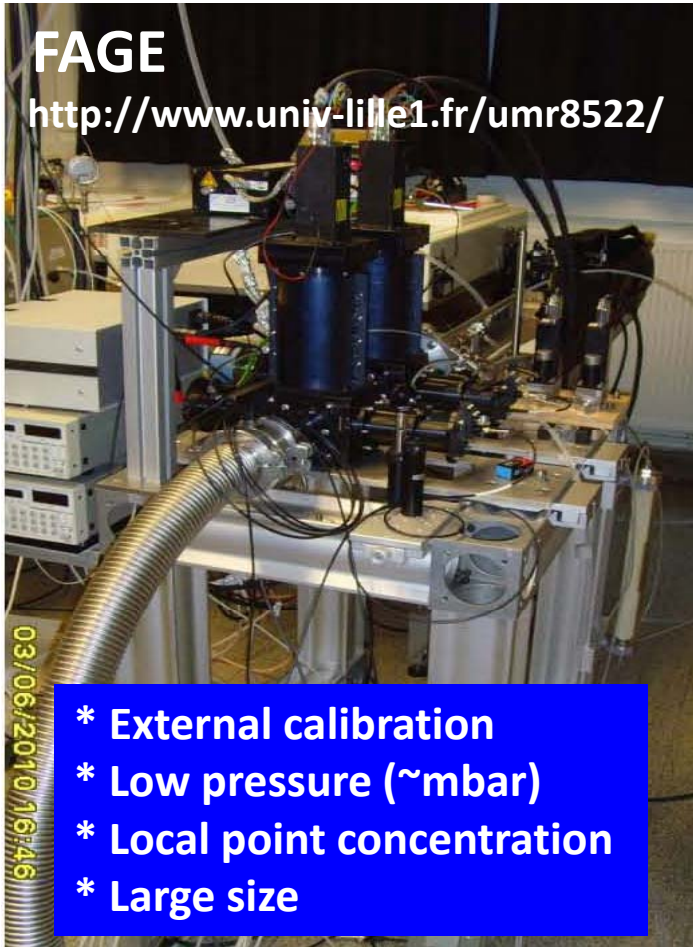

* External calibration
* Low pressure (~mbar)
* Local point concentration
* Large size

OH radical monitoring

Needs of compact instrument for self-calibration, direct concentration assessment with high spatial resolution & fast temporal response

WMS enhanced OA-ICOS @ 1434 nm

(WMS lowering noise / cavity enhancing signal)

FRS @ 2.8 µm

(shot noise dominated detection)

Production & calibration of OH radicals

The OH free radical was produced by **microwave (MW) discharge** in water vapor. The generated OH concentration was determined with the help of **wavelength modulation spectrum using a close-by H_2O absorption line**.

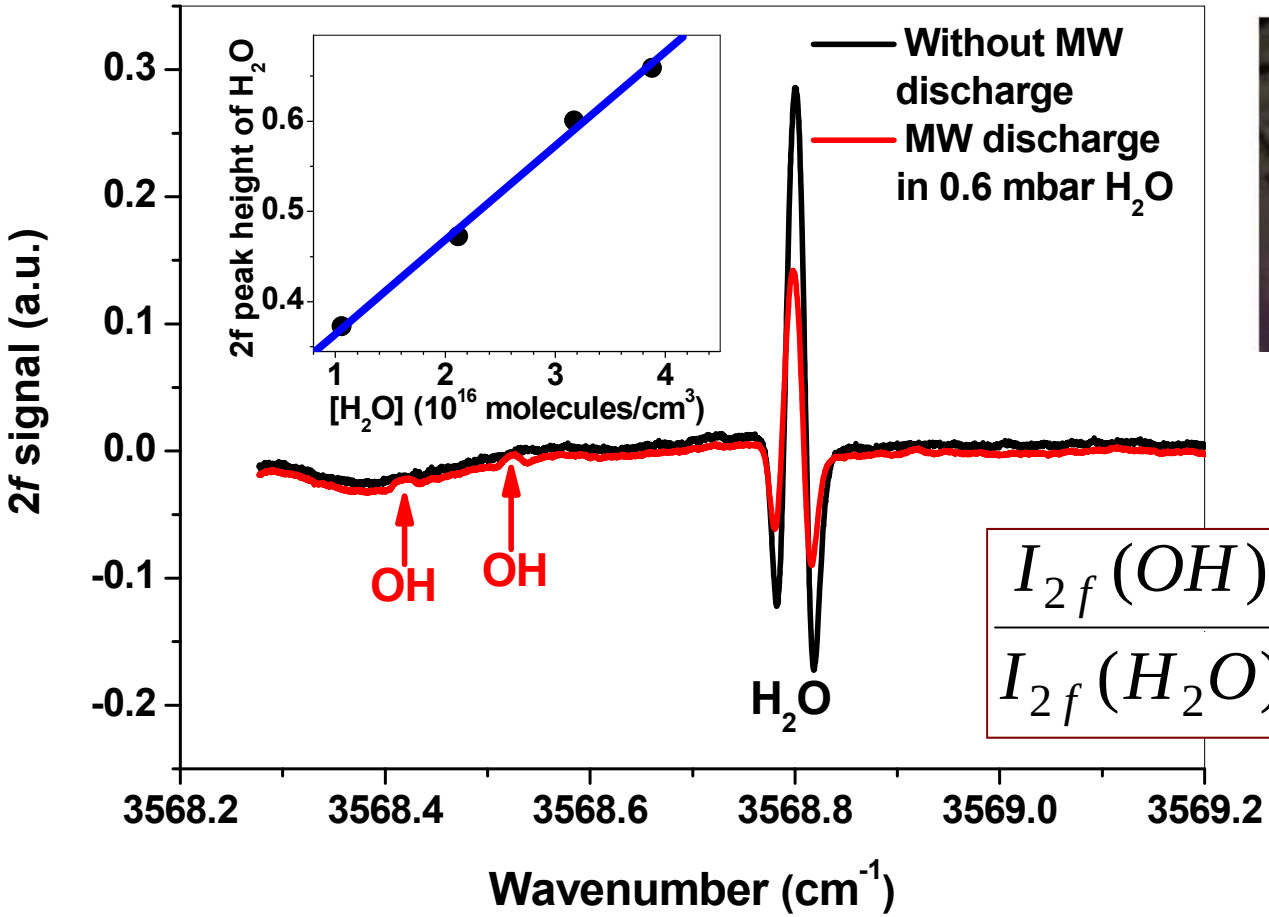

$$\frac{I_{2f}(OH)}{I_{2f}(H_2O)} = \frac{[OH]\times S_{OH}}{[H_2O]\times S_{H_2O}}$$

OH radical monitoring by

WMS enhanced OA-ICOS @ 1434 nm

(WMS lowering noise / cavity enhancing signal)

Cavity Enhanced Absorption Spectroscopy (CEAS)

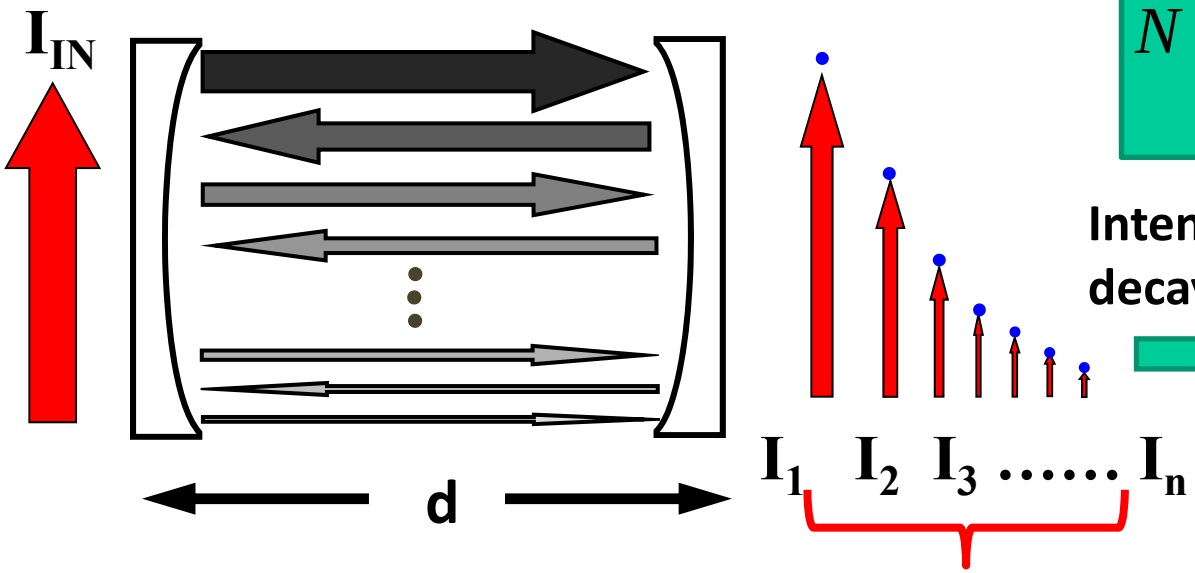

$$N = \frac{1}{c\sigma(\lambda)} \times \left(\frac{1}{\tau} - \frac{1}{\tau_0} \right)$$

Intensity decay rate

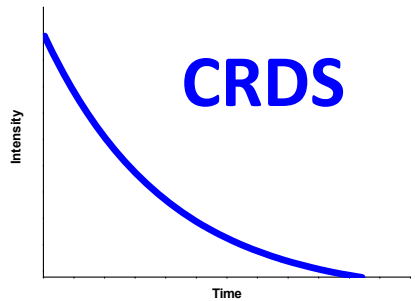

CRDS

$$I_{OUT} = \sum_n I_n$$

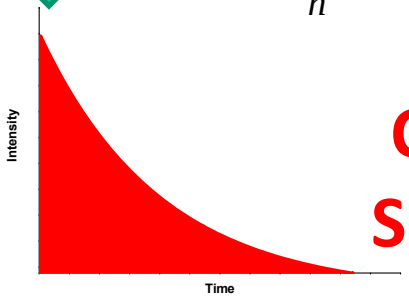

$$N = \frac{1 - R(\lambda)}{\sigma(\lambda) \times d} \left(\frac{I_0(\lambda)}{I(\lambda)} - 1 \right)$$

« Integrated Cavity Output Spectroscopy »

Calibration: determination of the mirror reflectivity R

$$N = \frac{1-R(\lambda)}{\sigma(\lambda)\times d}\left(\frac{I_0(\lambda)}{I(\lambda)}-1\right)$$

ICOS is not an absolute technique : R (λ) to be known

Cavity physical length

Experimentally measured spectrum

R(λ) can be determined by measuring :

- absorber with known concentration [Environ. Sci. Technol. **40** (2006) 6758] ;
- Rayleigh scattering difference of two species (e.g. He and Zero air) [Atmos. Chem. Phys. **8** (2008)7779] ;
- calibrated low-loss of an optical substrate [Appl. Opt. **48** (2009) B159] ;
- phase shift CRDS [Rev. Sci. Instrum. **79** (2008) 123110] ;

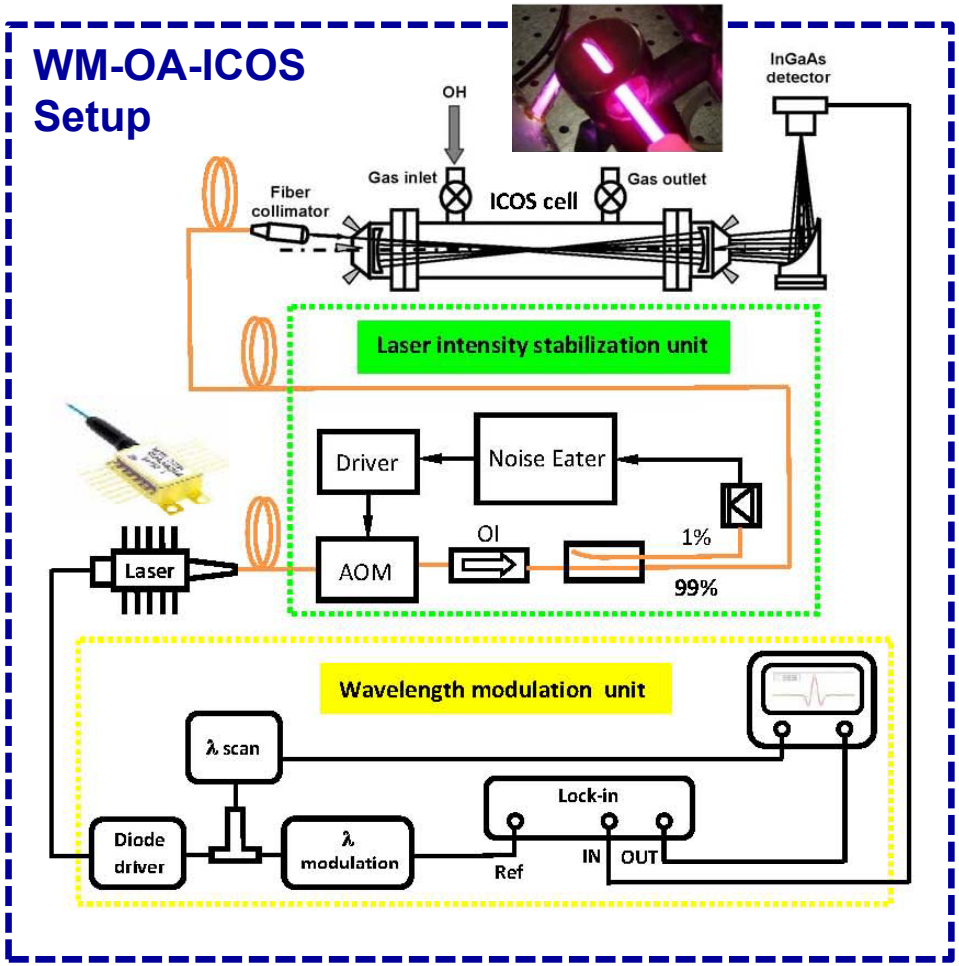

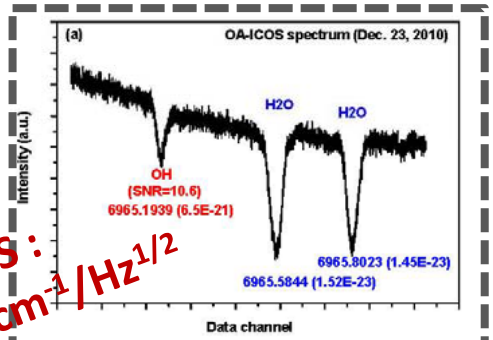

NEAS : 1.0×10^{-10} $cm^{-1}/Hz^{1/2}$

OH line at 6965.19 cm^{-1} with a line intensity of 6.5 × 10^{-21} $cm^{-1}/(molecule.cm^{-2})$

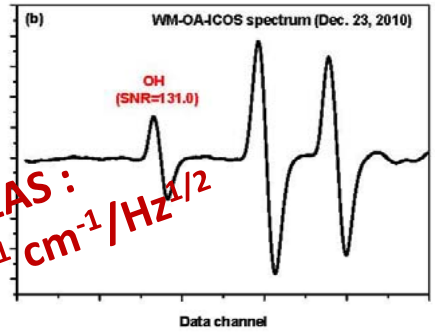

NEAS : 2.7×10^{-11} $cm^{-1}/Hz^{1/2}$

WM enhanced OA-ICOS detection sensitivity by a factor of ~ 12 in SNR.

Using OA-ICOS with an effective absorption path length of L_{eff} of ~ 1.2 km => DL of

~ 5×10^{9} OH/cm^{3}

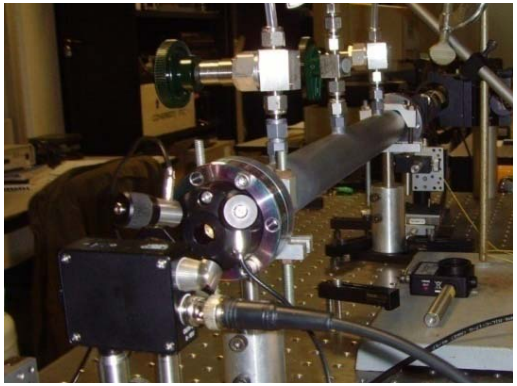

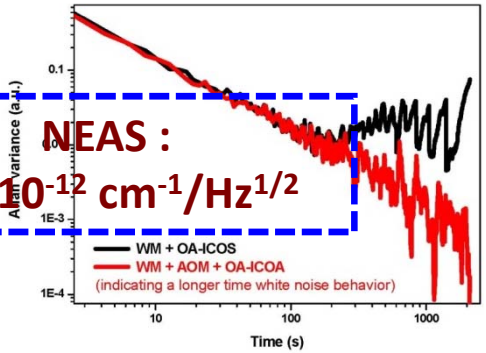

NEAS : 4.5×10^{-12} $cm^{-1}/Hz^{1/2}$

OH radical monitoring by

FRS @ 2.8 µm

(shot noise dominated detection)

Faraday Rotation Spectroscopy (FRS)

The FRS relies on the particular magneto-optic effect observed for paramagnetic species (OH, HO_2, CH_2O, NO, O_2, NO_2, etc.) : Interaction of incident laser beam with the paramagnetic species under a magnetic field results in a rotation of the polarization plane of a linearly polarized laser beam => **FRS signal P(φ)**

$$P(\varphi) = \frac{P_0}{2}(1 - \cos 2\varphi + R_\Delta L \sin 2\varphi)$$

and $R_\Delta = k_0(n_+ - n_-)$, **responsible for creation of the FRS signal***

The FRS signal depends on :

- ✓ **Molecular line strength, S**
- ✓ **Optical path length, L**
- ✓ **The rotational gyromagnetic ratio g-factor, g**
- ✓ **Magnetic field strength, B**
- ✓ **Molecule concentration, C**

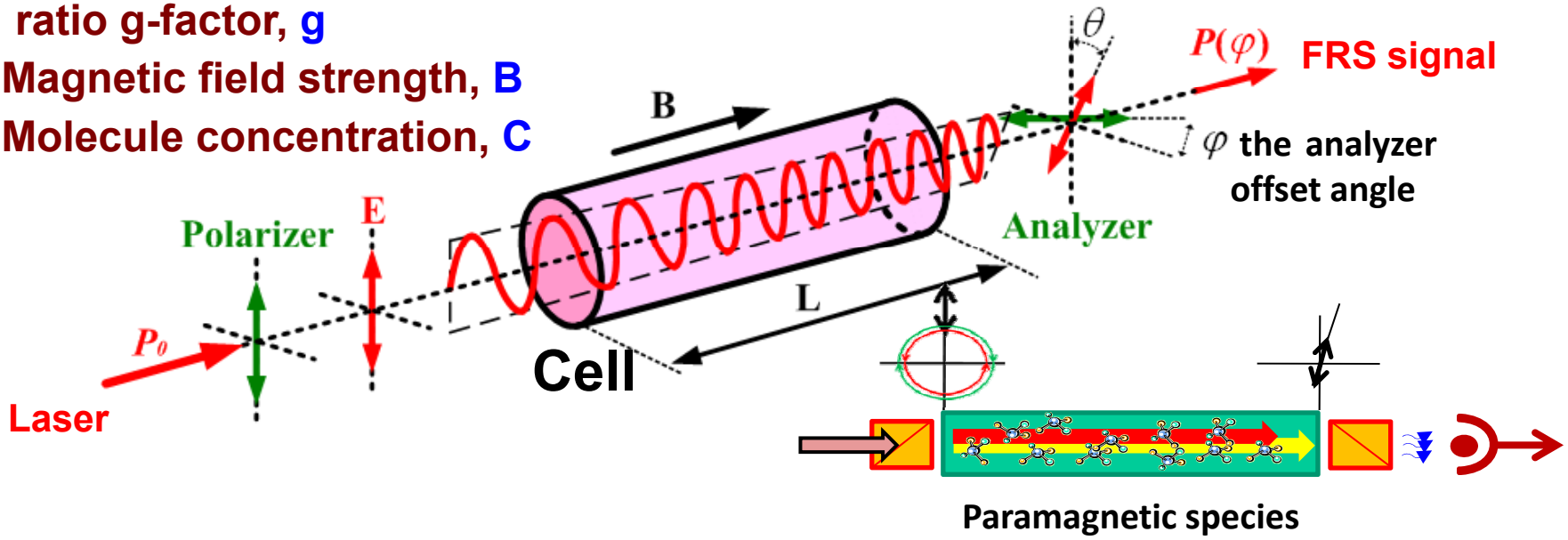

Merits of FRS

FRS strongly enhances the detection sensitivity and selectivity:

⇒ **Detection of Faraday rotation effect provides selectivity to paramagnetic species. No interference from diamagnetic species (CO_2, H_2O) in the atmosphere ;**

⇒ **Two nearly crossed polarizers with high extinction ratio provide significant reduction of the laser source noise ;**

⇒ **Internal sample modulation through molecular Zeeman energy split provides excellent suppression of all external noise (like stray modulation and most importantly interference fringes).**

OH monitoring by FRS @ 2.8 μm

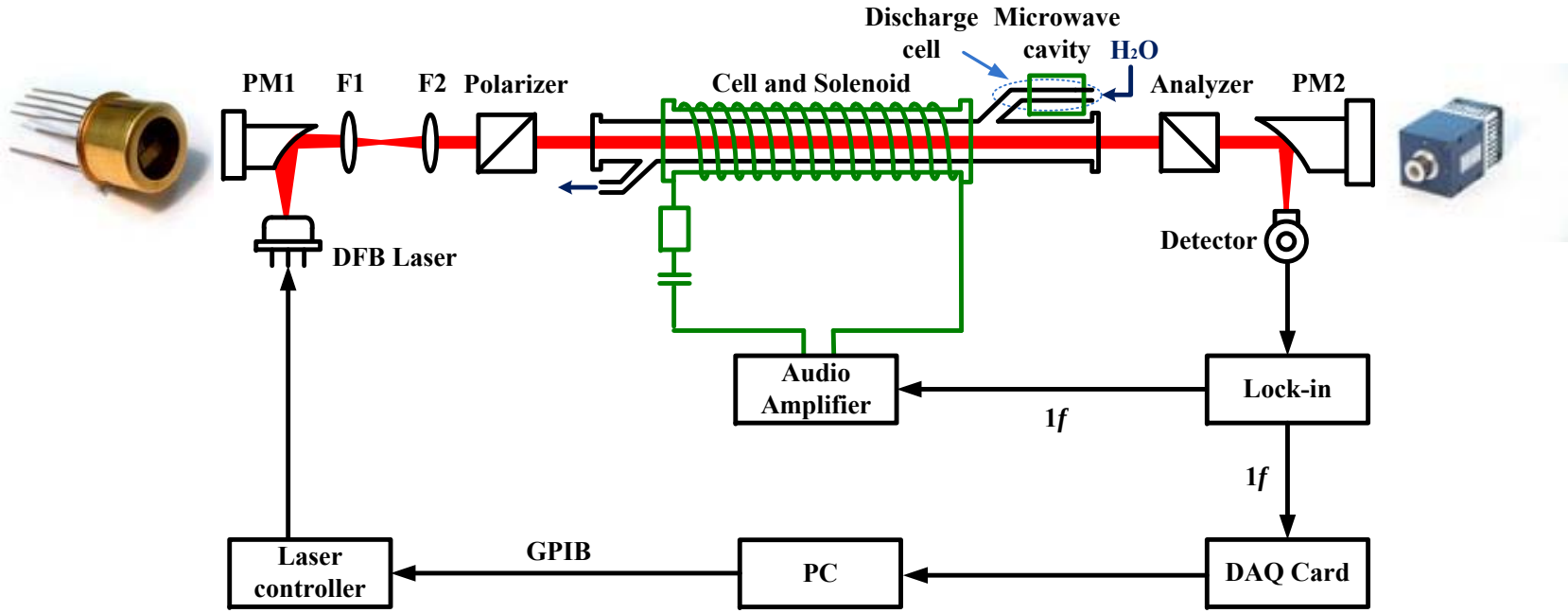

Zhao et al., Opt. Express 19 (2011) 2493-2501 & Appl. Phys. B 109 (2012) 511-519

RT DFB diode laser at 2.8 μm (nanoplus GmbH)

- Single-mode tuning range : ~ 5 cm^{-1}
- CW laser emission power : ~ 2 mW
- λ-tuning coefficients: 0.05 nm/mA & 0.25 nm/K

Polarizers : high extinction ratio of $\xi < 5 \times 10^{-6}$

Solenoid : 25 cm long, operating in AC mode at a resonant frequency of 1.302 kHz, with a magnetic field of B ~ 95 $Gauss_{rms}$

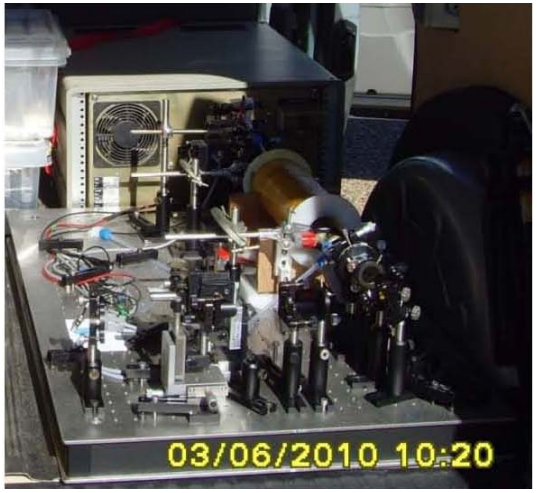

Shot-noise dominated detection of OH radical

System noise $N_{tot}(\varphi) = \sqrt{N_0^2 + N_1^2(\sin^2(\varphi)+\xi) + N_2^2(\sin^2(\varphi)+\xi)^2}$

- The **shot noise N_1** = 4.897 ± 0.292 μV Hz$^{-1/2}$
- The **laser noise N_2** = 3.298 ± 1.152 μV Hz$^{-1/2}$
- The **detection system noise N_0** = 0.433 ± 0.019 μV Hz$^{-1/2}$

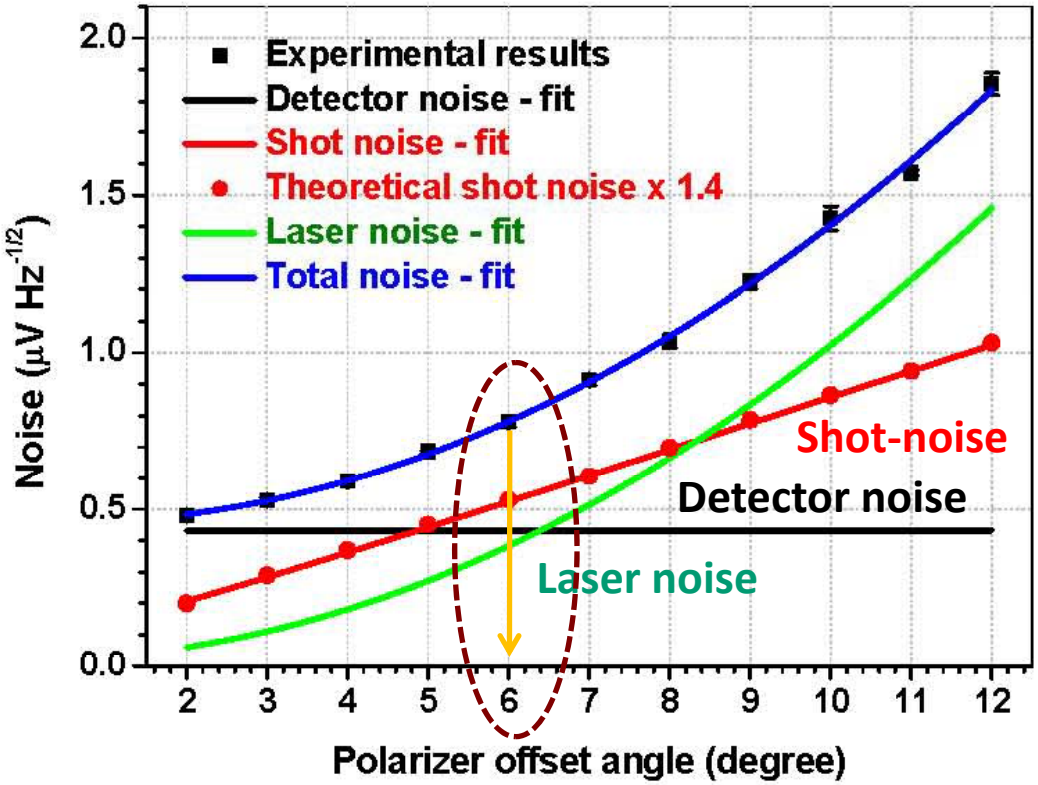

- The total noise at φ_{opt} = 6°:

  0.78 μV Hz$^{-1/2}$

- Operation at **~ 2× theoretical shot-noise** of **0.38 μV/Hz$^{1/2}$**
- A minimum detectable Faraday rotation angle:

  1.39 × 10^{-7} rad Hz$^{-1/2}$

- **System noise is shot-noise predominated**

OH monitoring by FRS

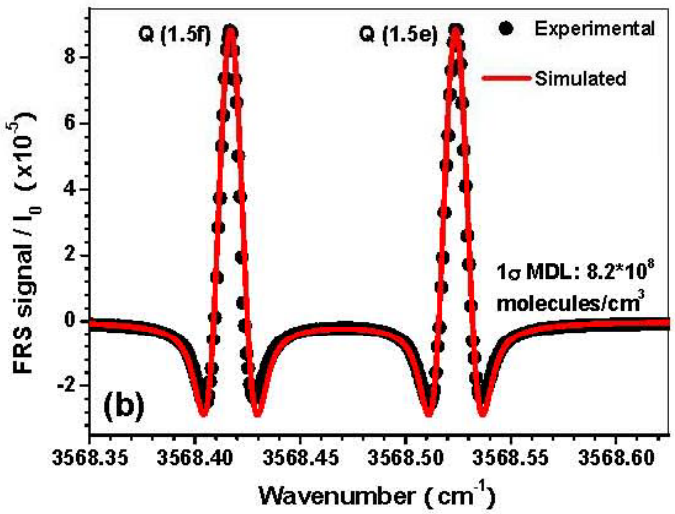

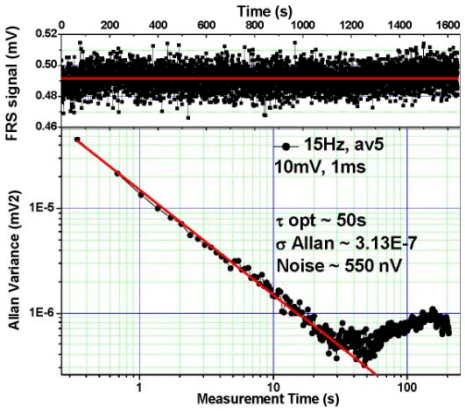

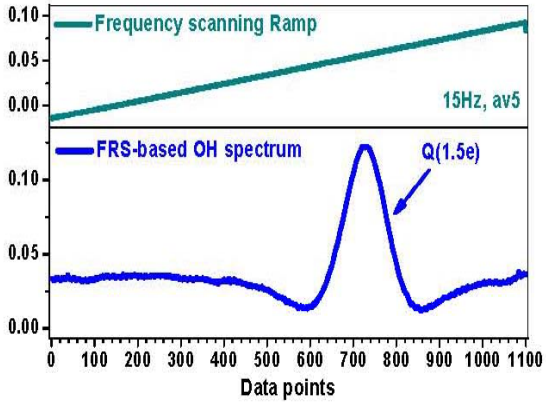

Point-by-point frequency tuning mode

1σ MDL : **8.2×10^8 OH/cm^3** in a 25-cm long single pass cell (lock-in time =100 ms)

Fast scanning mode

1σ MDL : ~ **5.5×10^8 OH/cm^3** in a 25-cm long single pass cell.

(Scan rate : 15 Hz & average time : 50 s)

The prototype instrument shows high potential for field applications: compact, self-calibration, direct concentration assessment. Longer absorption pathlength approach to be implemented to lower the minimum detection limit (~ 10^6 OH/cm^3).

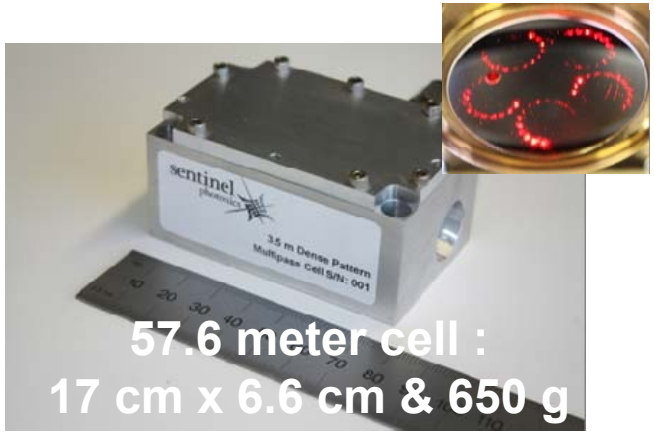

HONO detection

Lifetimes: ~ a few minutes
Environment: ~ ppbv / indoor: ~10 ppbv / in car: tens of ppbv

HONO is a very important source of the OH radical. Recent researches show that the photolysis of HONO accounts for up to 60% of the integrated OH radical source strengths (*Nature* 440 (2006) 195-198). Modeled HONO concentrations are often significantly below field observed values, which suggest a large missing source of HONO (*Science 333 (2011) 1616-1618*) ….

Campaigns: PRIDE-PRD 2004 (China), BEARPEX 2007 (California), DOMINO 2008 (Spain), CINDI 2009 (The Netherlands), SHARP 2009 (Houston), CalNex 2010 (California), FIONA 2010 (Spain), ….

Needs to better understand the contribution of HONO to the atmospheric photochemical processes and the OH budget

Quantitative analyses of HONO

Accurate and precise *in situ* assessment of HONO concentration is hence highly desirable. Quantitative analysis of HONO is usually made **in the aqueous phase** after wet chemical conversion or **in the gas phase** using spectroscopic techniques.

Chemical instruments (denuder, mist chamber or stripping coil + IC, FL, CL, LOPAP, HPLC) : typically **cheap**, **easy to use** and very **sensitive** (down to ~ pptv) with a time resolution of minutes to hours. Unquantified **chemical interferences** and **sampling induced artifacts**. Validation and calibration of chemical instruments against spectroscopic instruments are of paramount importance.

Spectroscopic instruments (TDLS, IBBCEA, DOAS) : **free of sampling artifacts & chemical interference**, **self-calibration**.

HONO generation & quantification

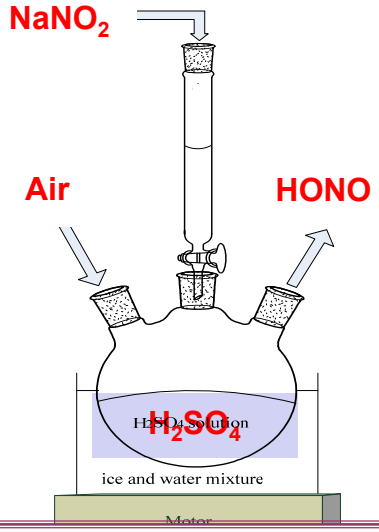

QCL sensor

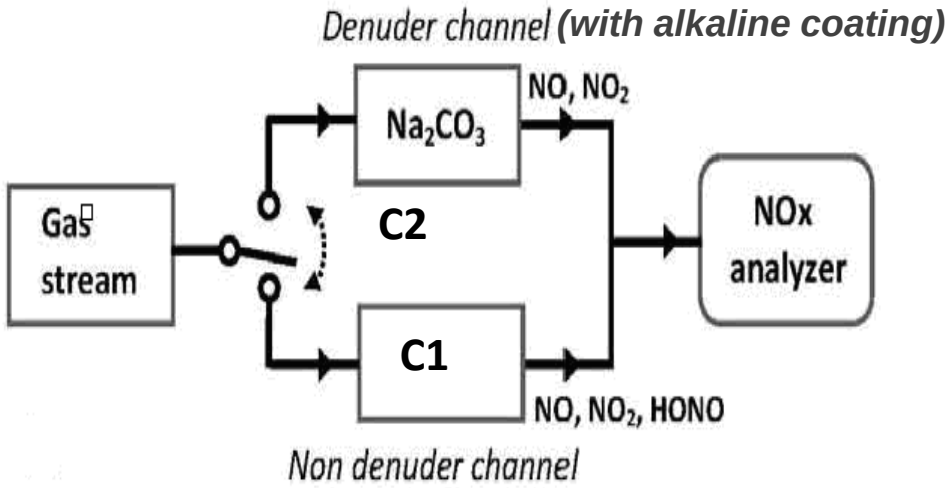

$NaNO_2 + H_2SO_4 = NaHSO_4 + HONO$

$HONO \leftrightarrow NO + NO_2 + H_2O$

C1= [NOx] + [HONO] + Adsorption losses

C2 = [NOx] + Adsorption losses

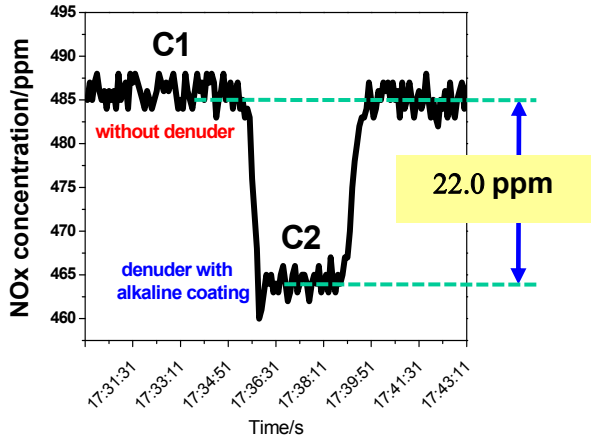

[HONO] = C1 – C2

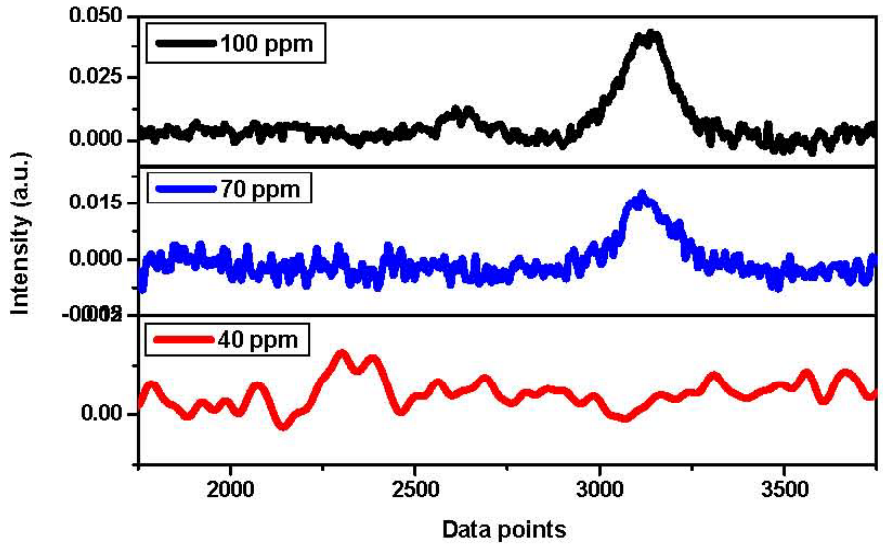

QCL-based HONO Sensor

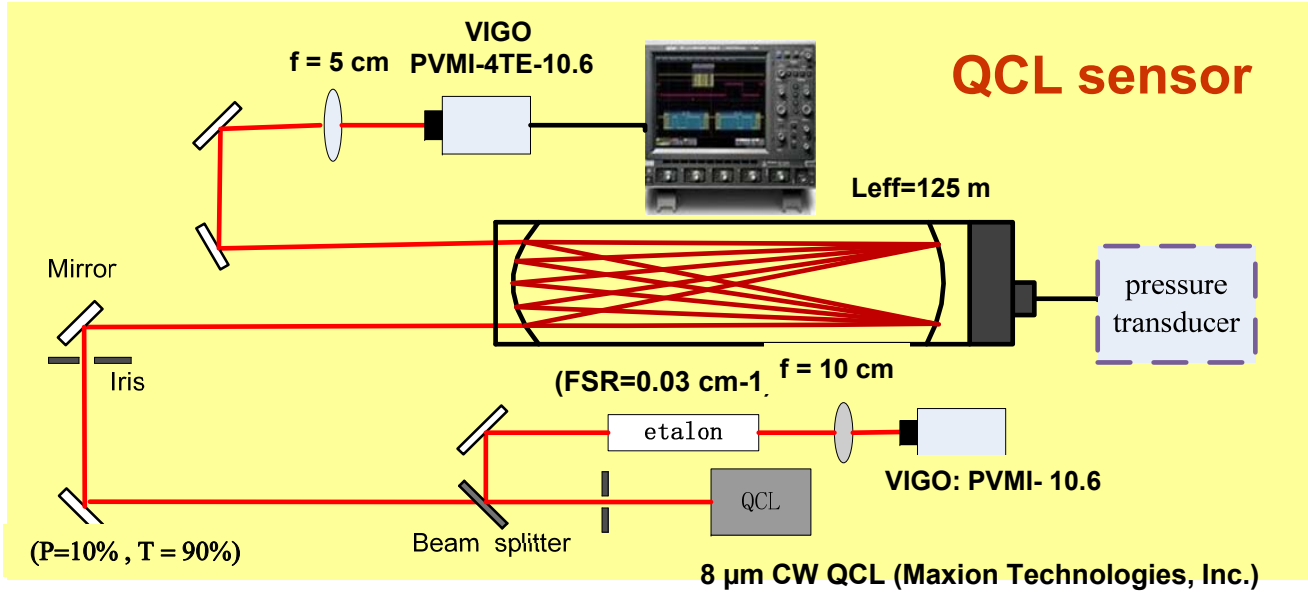

1σ det. Sen. (1 s) :
HONO : < 400 ppt
CH4 : 4 ppb

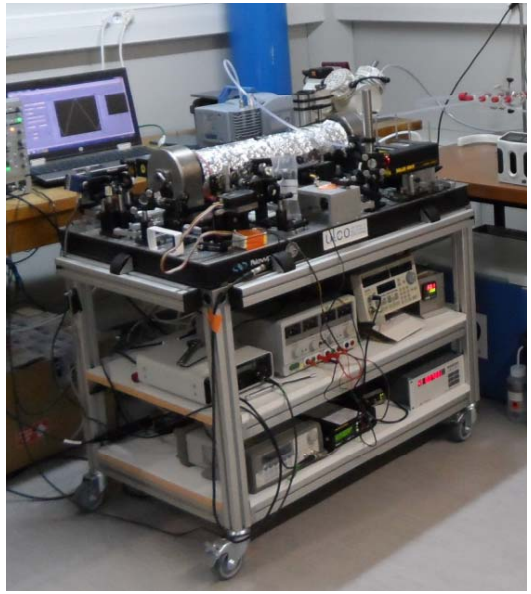

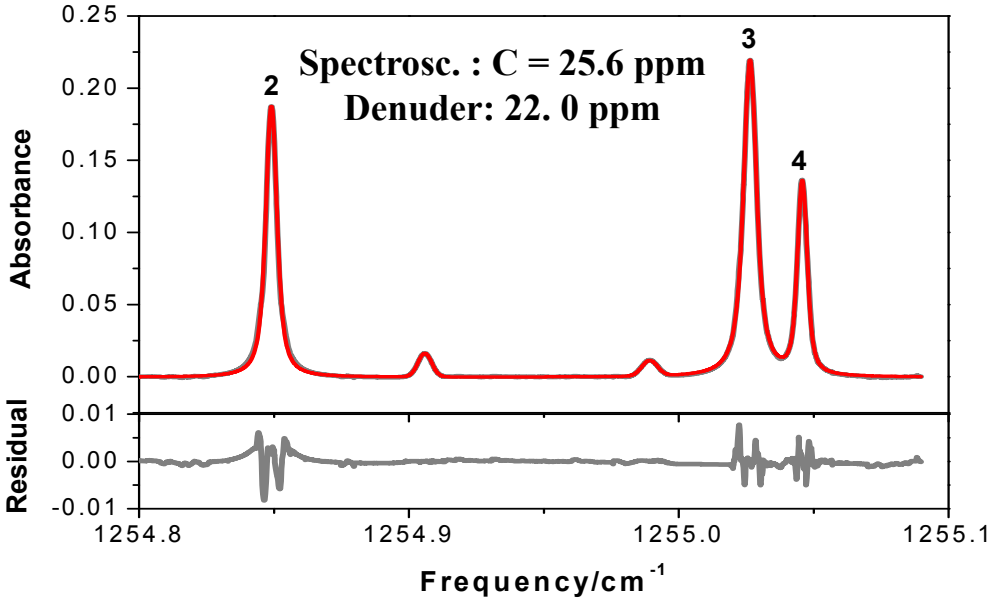

Sensing by Light Emitting Diodes (LED)

HONO, NO_2 &NO_3 radical monitoring

Structured absorptions in the visible and UV spectral region (fdl electronic transition)

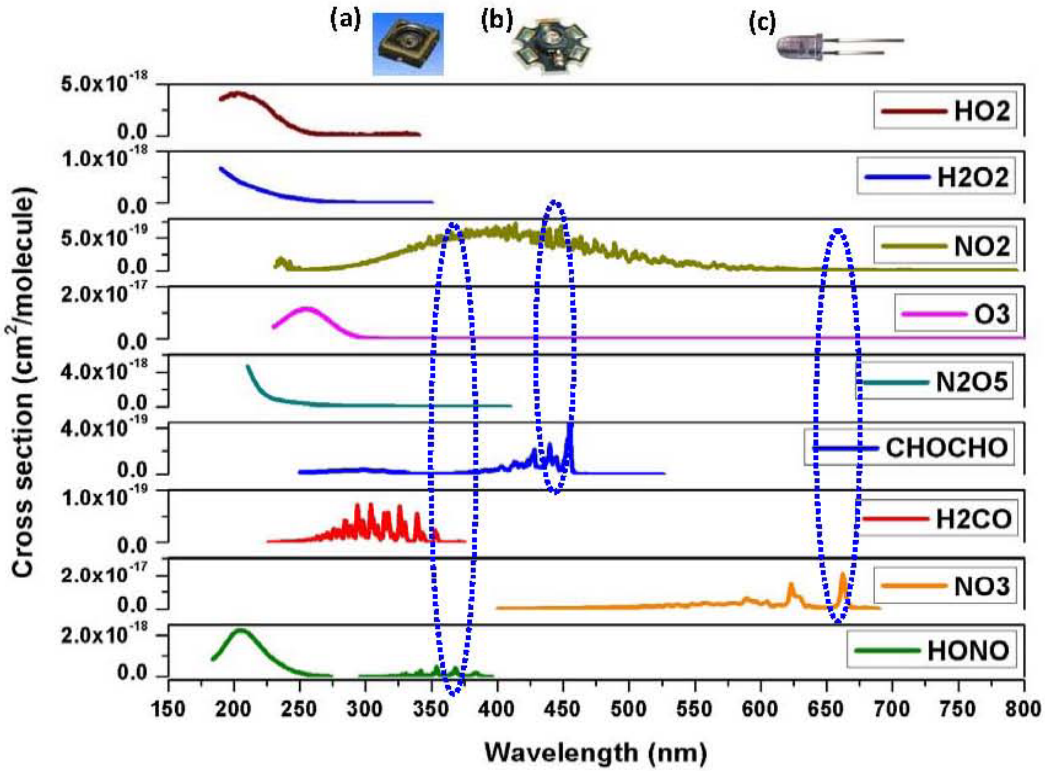

	(a) NCSU033AT (NICHIA)	(b) LXHL-LR3C (LUMILEDS)	(c) SMB660N (USHIO)
Optical power	250 mW (@ 500 mA)	340 mW (@ 700 mA)	300 mW (@ 500 mA)
Peak wavelength	365 nm	455 nm	660 nm
Bandwidth (FWHM)	18 nm	20 nm	25 nm
Viewing ½ angle	± 20°	± 70°	± 7°
lifetime	~ 100 000 hr		
Cost per LED	$60	$8	$8
Target molecules	HONO / NO2 [1] CH2O	NO2 / CHOCHO [2]	NO3 / NO2 [3]

[1] T. Wu, W. Chen, E. Fertein et al., Appl. Phys. B **106** (2012) 501–509
[2] T. Wu, W. Zhao, W. Chen et al., Appl. Phys. B **94** (2009) 85–94
[3] T. Wu, C. Coeur, G. Dhont et al., EST (2013)

Strong and structured broadband molecular absorptions in the VIS and UV regions, arising from the fdl electronic transition, allow for high sensitivity detection of multiple key atmospheric species at the ppbv-pptv levels.

Sensitive spectroscopic approaches in the VIS and UV

Differential Optical Absorption Spectroscopy (DOAS)

- ✓ Long pathlength absorption (~ km)
- ✓ Using broadband light for multiple species detection
- ✓ Low spatial resolution - Cumbersome (L_{Base} ~ km)

Cavity Ringdown Spectroscopy (CRDS)

- ✓ Cavity enhanced long effective pathlength (~ km)
- ✓ High spatial resolution - Compact (L_{Base} ~ m)
- ✓ Narrow laser spectral coverage, limited for multi-species detection

Broadband Cavity Enhanced Spectroscopy (BBCEAS)

- ✓ Cavity enhance (high spatial resolution for reactive species) :

  => Long effective pathlength (~ km) & Compact (L_{Base} ~ m)

- ✓ Broadband light => Simultaneous multi-species measurement

Open path IBBCEAS of HONO & NO_2 detection @ 365 nm

No wall losses or heterogeneous production of HONO

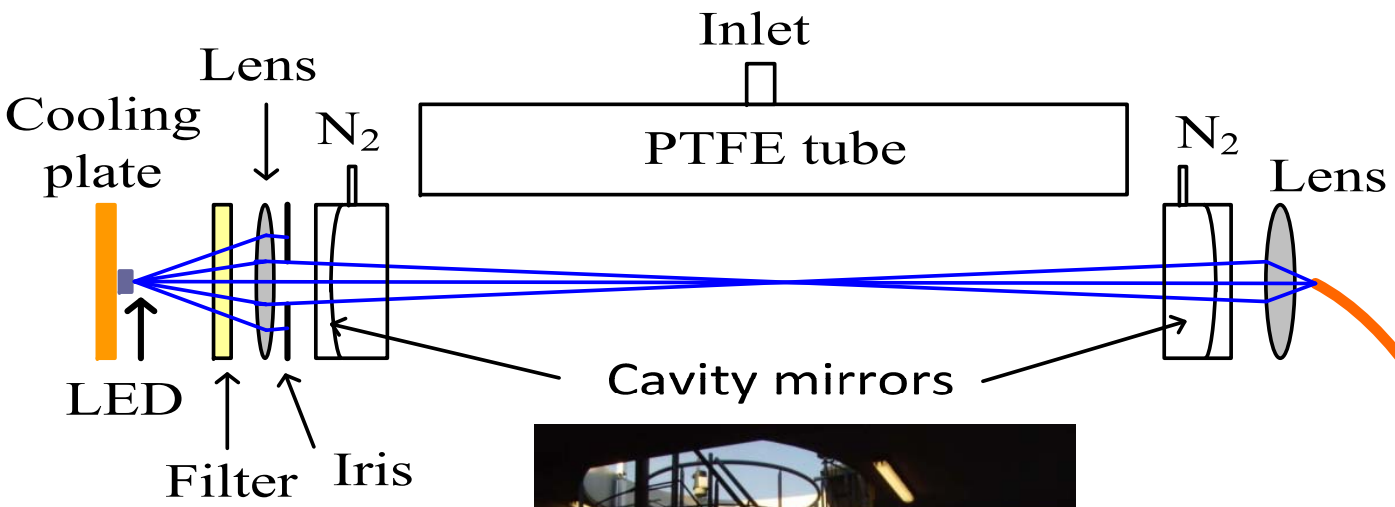

1 σ MDC (90 s) :
HONO : 430 pptv
NO_2 : 1 ppbv

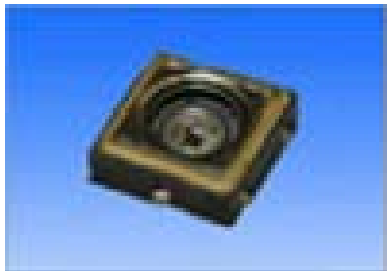

Wu et al., Appl. Phys. B106 (2012) 501–509

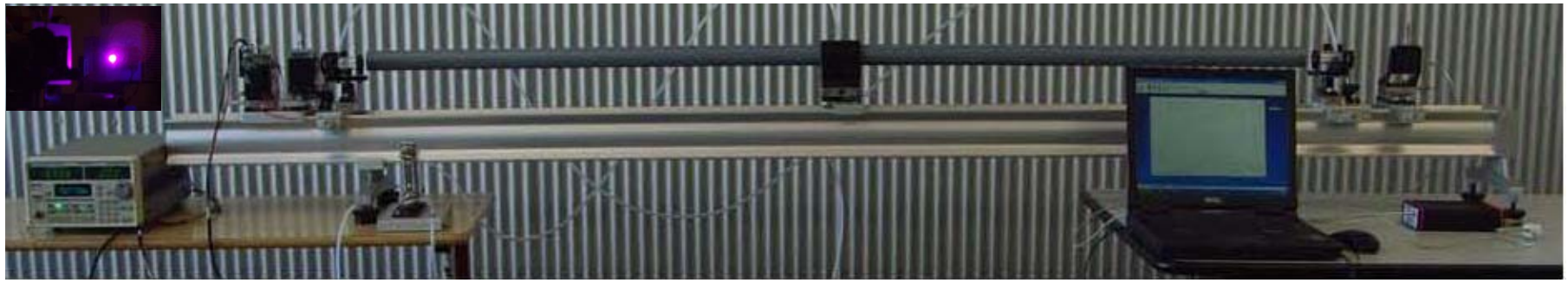

Simultaneous concentration retrieval of multiple species

Nonlinear least-square fitting based on the Levenberg-Marquardt algorithm

Polynomial function for slow variations with wavelength:
(1) baseline
(2) Rayleigh & Mie scattering

Known after calibration

$$\alpha(\lambda) = n_{HONO}\sigma_{HONO}(\lambda) + n_{NO2}\sigma_{NO2}(\lambda) + a_0 + a_1\lambda + a_2\lambda^2 = \frac{1-R(\lambda)}{d} \times \left(\frac{I_0(\lambda)}{I(\lambda)} - 1\right)$$

Reference spectra

Cavity physical length

Experimentally measured spectrum

Target species concentrations can be simultaneously retrieved by a multivariate fit

Simultaneous measurement of HONO and NO_2

(using multivariate fit of ref. σ to exp. spectrum)

$$\frac{1-R(\lambda)}{d}\left(\frac{I_0(\lambda)}{I(\lambda)}-1\right)=n_{HONO}\,\sigma(\lambda)_{HONO}+n_{NO2}\,\sigma(\lambda)_{NO2}+a_0+a_1\lambda+a_2\lambda^2$$

Exp. spectrum **Ref. σ(λ)** **Baseline**

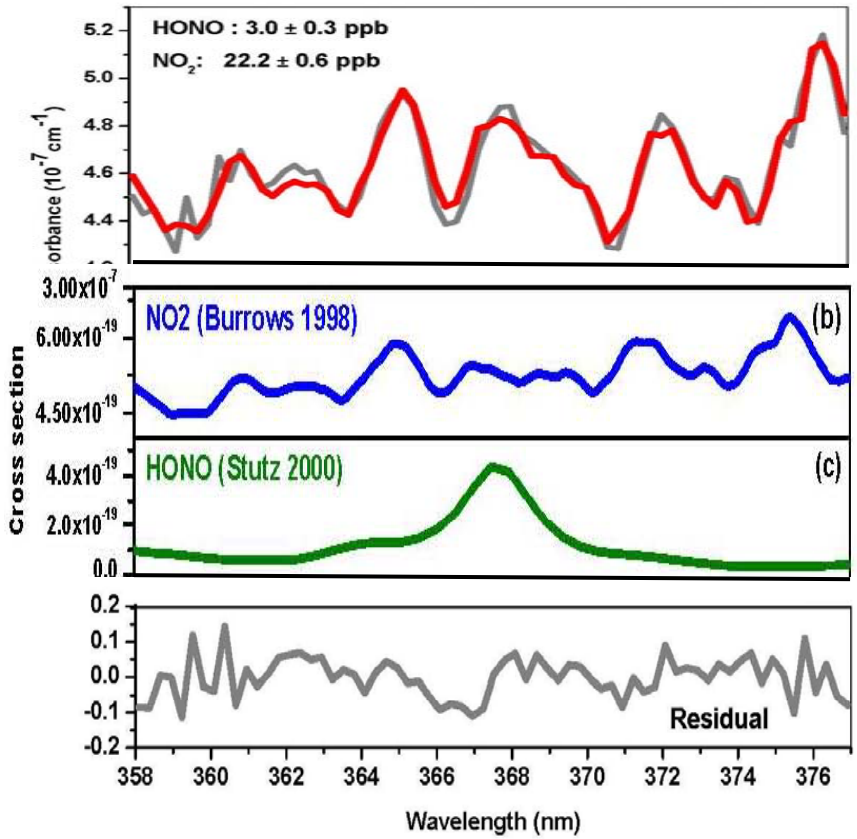

Determination of the cavity mirrors' reflectivity: R(λ)

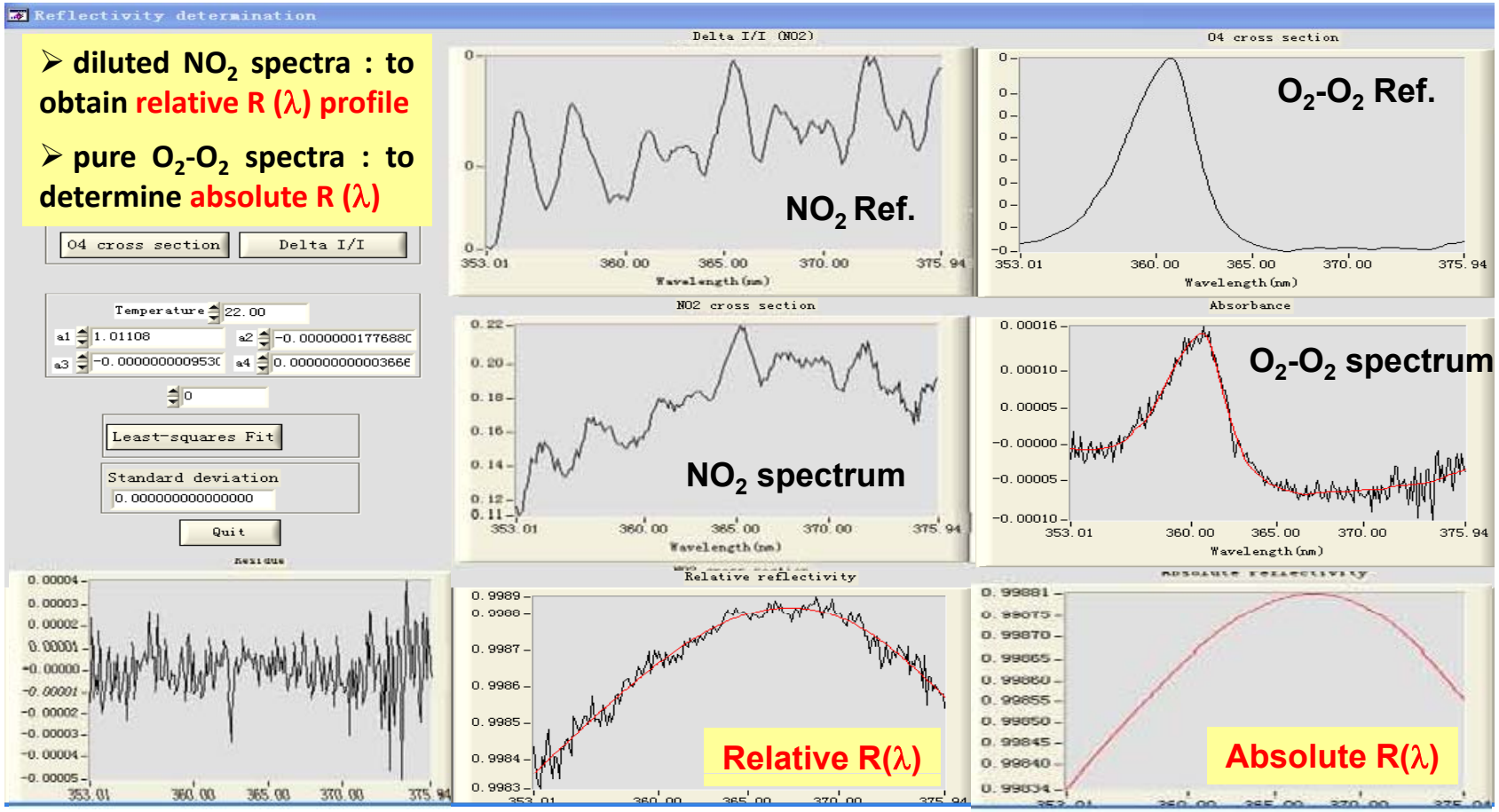

By using measured absorption spectra of 100 ppbv NO_2 (generated with a gas dilution calibrator, Sabio instruments) and pure O_2, the max. cavity mirror's reflectivity was determined to be ~0.99916, which corresponded to an effective pathlength of ~2.1 km (based on a cavity length of L=1.76 m).

Applications

- Field observation of HONO & NO_2 in sub-urban @ 356 nm 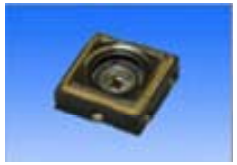

- NO_2 & NO_3 radical monitoring for kinetic study in smog chamber @ 660 nm 

1) Field application in a Hong Kong Campaign

Hong Kong Polytechnic University & Environmental Protection Department of Hong Kong

Tung Chung

(sub-urban site)

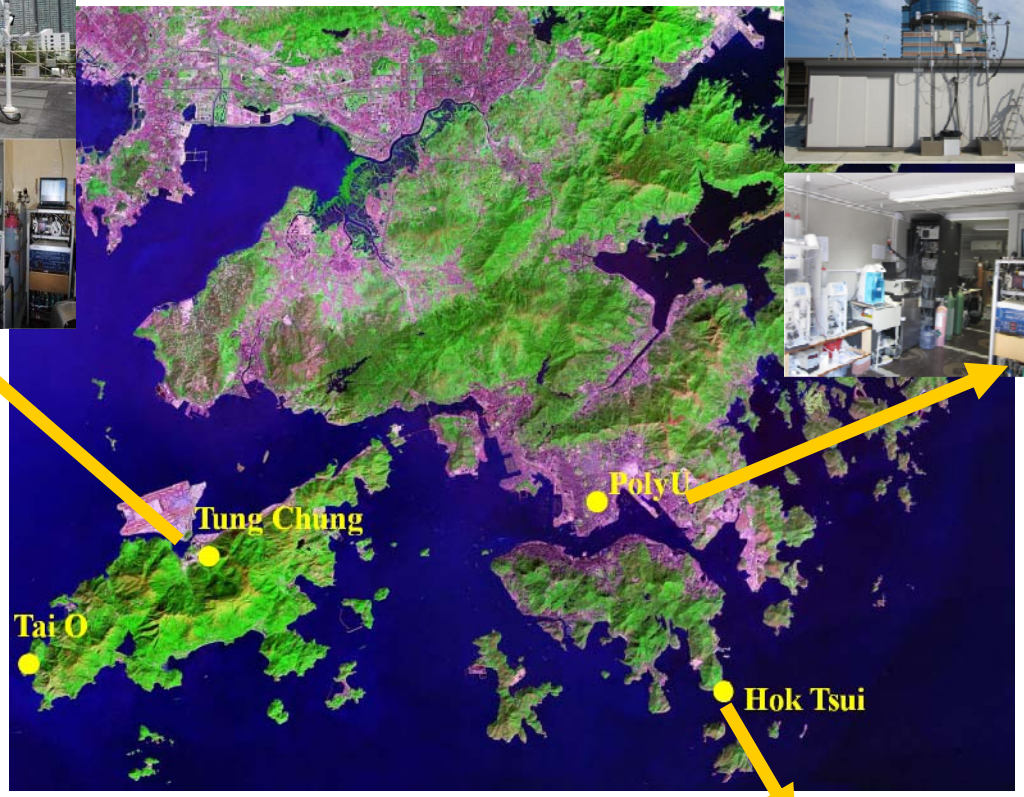

Poly U

Long-term background site on south-eastern Hong Kong Island (since 1993)

HONO : IBBCEAS vs. LOPAP

(HONO converted into color azo dye & det. in long path abs.)

NO_2 : IBBCEAS vs. BL-NOx analyzer

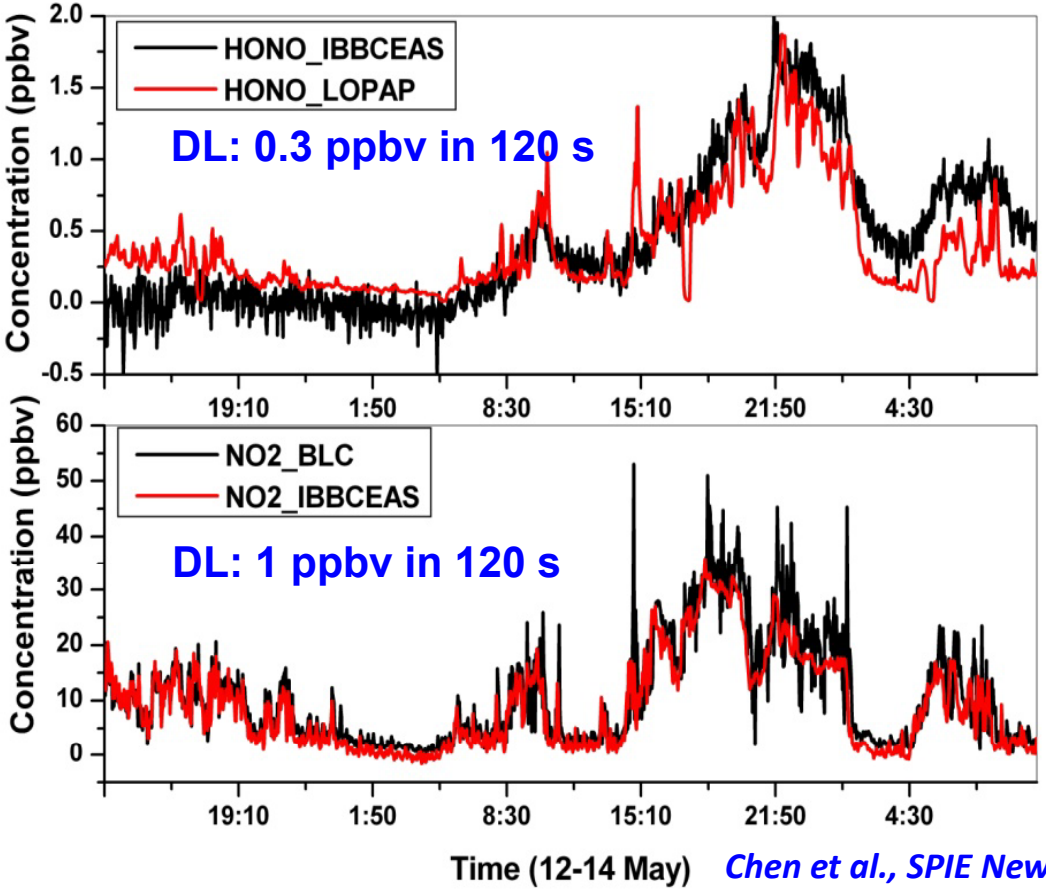

Detection sensitivity

1 σ detection limits (120 s) :

HONO: 300 pptv

NO_2 : 1 ppbv

Precision: < 10%

Chen et al., SPIE Newsroom (2013) DOI: 10.1117/2.1201301.004689

Time series of HONO and NO_2 concentrations measured by IBBCEAS, LOPAP and blue light (BL) based NOx analyzer at the TC site on 12-14th May 2012.

Field observation of HONO concentration variation

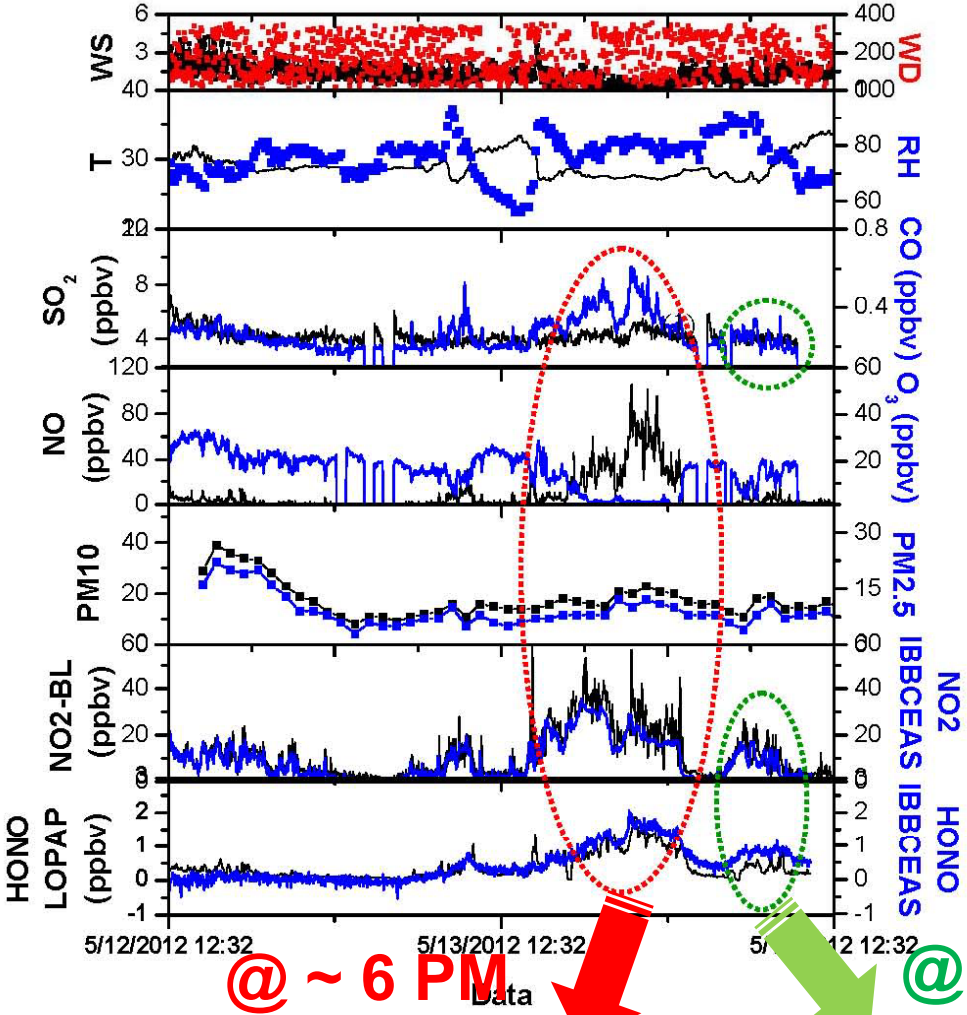

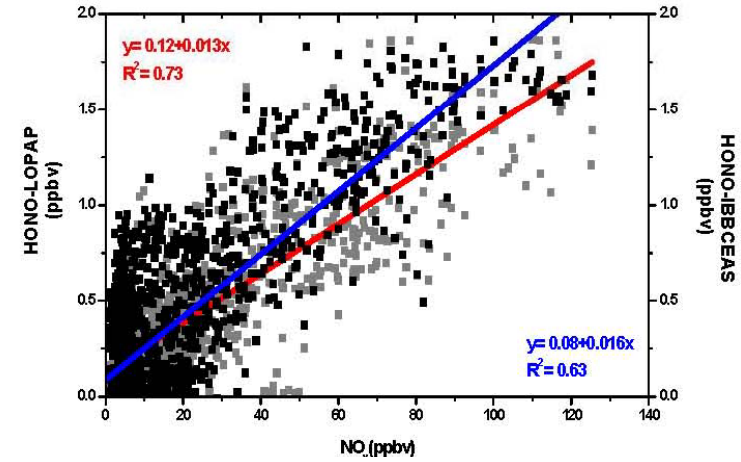

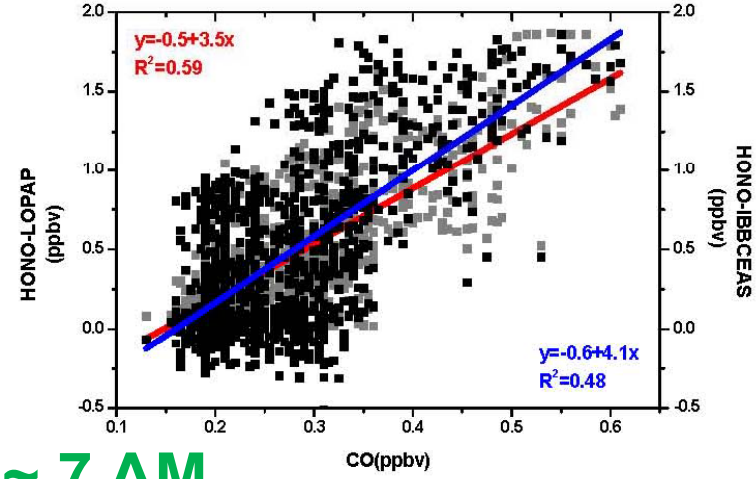

@ ~ 6 PM

CO combustion tracer
=> HONO from traffic emission

@ ~ 7 AM

Heterogeneous nighttime formation from NO_2 hydrolysis on surfaces

2) Monitoring NO_3 & NO_2 in a smog chamber

The most important nighttime oxidant with lifetimes: in seconds in daytime & in minutes in nighttime / Typical concentration : 5-400 ppt

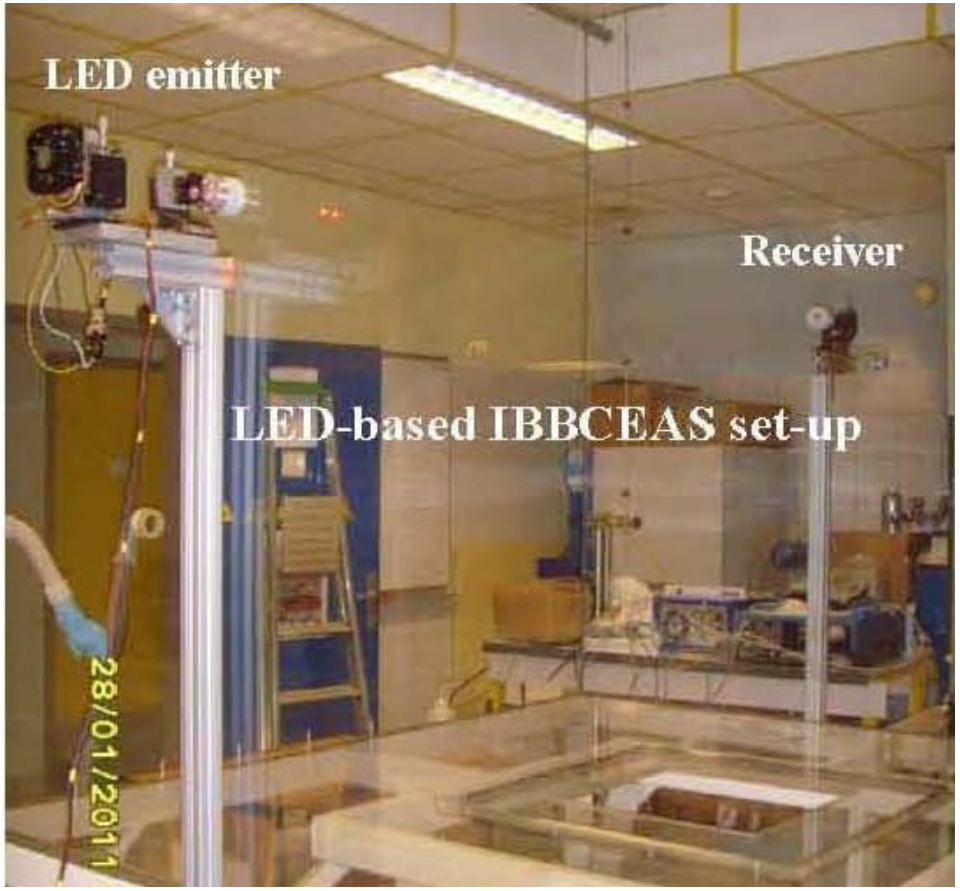

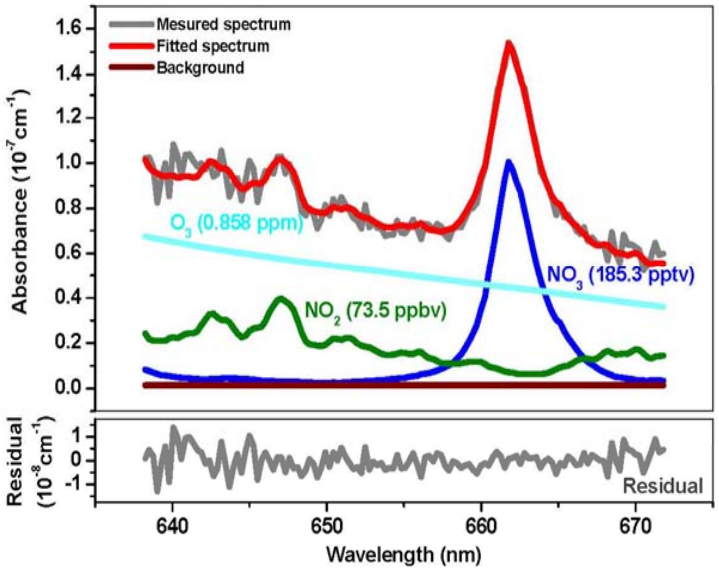

2 m X 2 m X 2 m in plexiglas, illuminated with 10 fluorescence tubes (400–800 nm, 40 W).

Real time monitoring photochemical processes in smog chamber

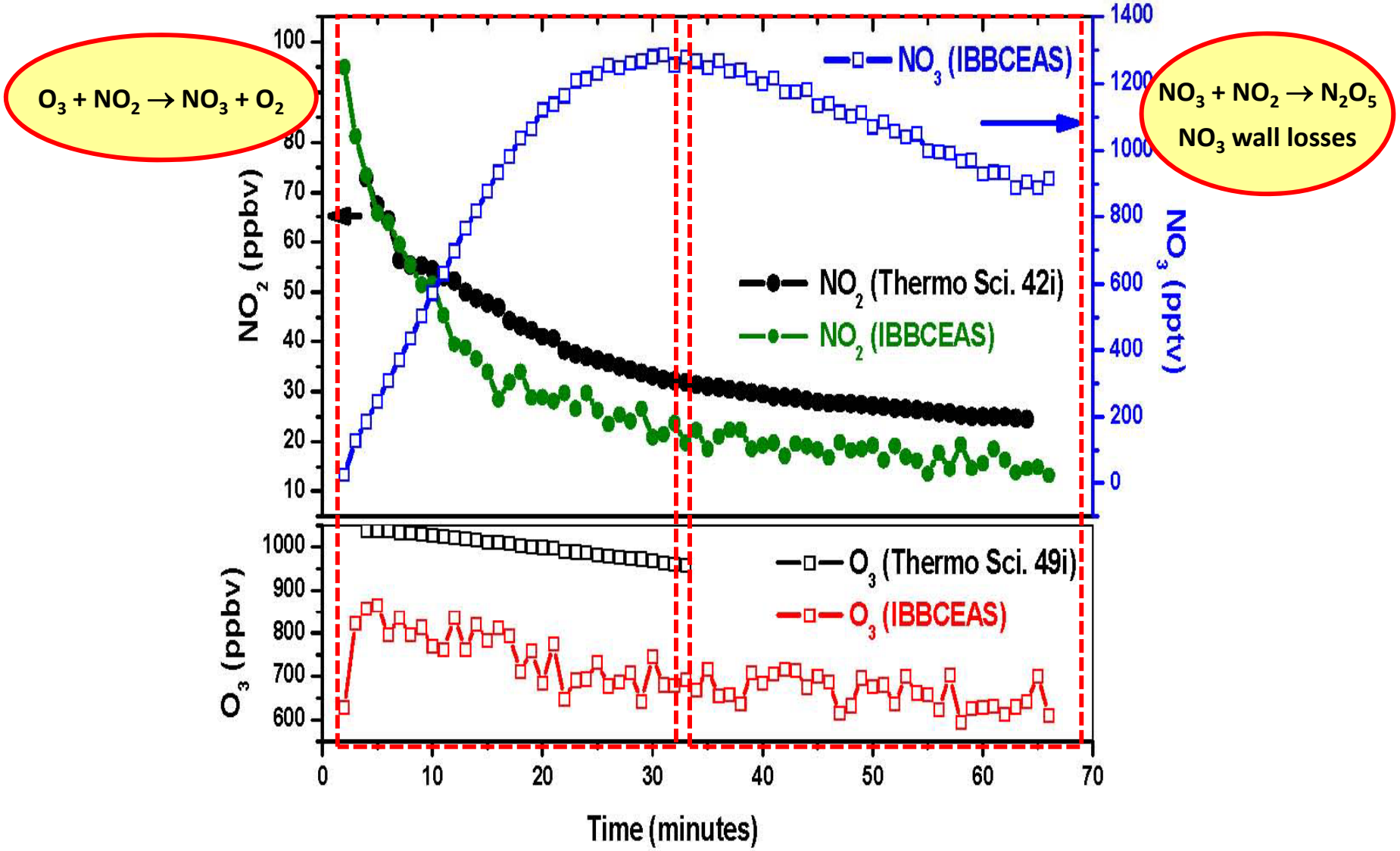

Temporal profiles of NO_3, NO_2 and O_3 concentrations measured by IBBCEAS (red) for kinetic study of the $NO_3 + NO_2 \leftrightarrow N_2O_5$ system to determine reaction rate constants

$$\frac{d[NO_2]}{dt} = -k_1[NO_2][O_3] - k_2[NO_2][NO_3] + k_3[N_2O_5],$$

$$\frac{d[NO_3]}{dt} = k_1[NO_2][O_3] - k_2[NO_2][NO_3] + k_3[N_2O_5] - k_4[NO_3],$$

$$\frac{d[N_2O_5]}{dt} = k_2[NO_2][NO_3] - k_3[N_2O_5].$$

Wu et al., EST (2013)

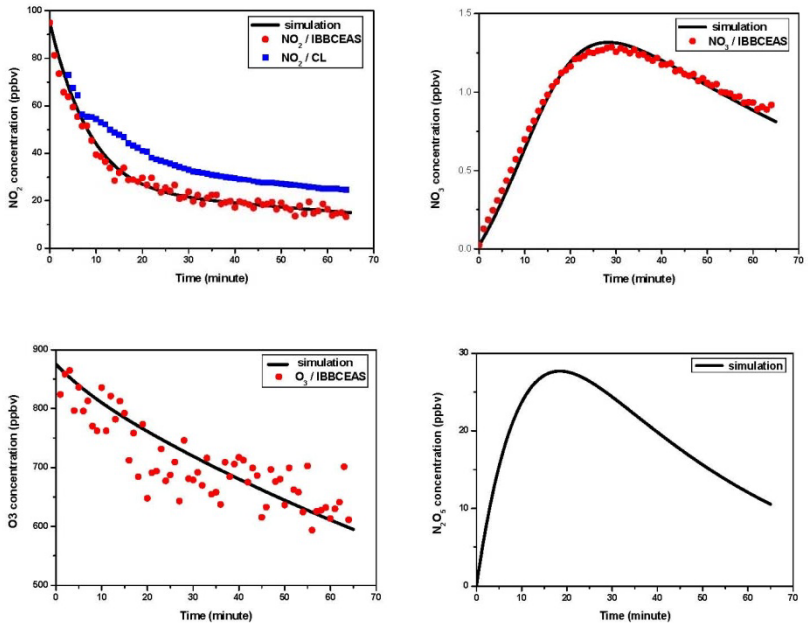

chemical reaction	constant	k (this work) at 296 K with k_2 fixed [a]	k (this work) at 296 K with k_{-2} fixed [a]	k (literature data) at 296 K
$NO_2 + O_3 \rightarrow NO_3 + O_2$	k_1 (cm^3 $molecule^{-1}$ s^{-1})	3.32×10^{-17}	3.31×10^{-17}	3.33×10^{-17} [a]
$NO_2 + NO_3 + M \leftrightarrow N_2O_5 + M$	k_2 (cm^3 $molecule^{-1}$ s^{-1})		1.19×10^{-12}	1.25×10^{-12} [a]
	k_{-2} (s^{-1})	3.62×10^{-2} s^{-1}		3.48×10^{-2} s^{-1} [a]
	K_{eq}			2.9×10^{-11} [b] 3.59×10^{-11} [c]
$NO_3 \rightarrow$ wall losses	k_3 (s^{-1})	1.53×10^{-2} s^{-1} [d]	1.53×10^{-2} s^{-1} [d]	
$O_3 \rightarrow$ wall losses	k_4 (s^{-1})	7.54×10^{-5} s^{-1} [d]	7.53×10^{-5} s^{-1} [d]	

[a] Recommended value at 296 K, Atkinson et al., 2004 (IUPAC-web version, 2004).
[b] Recommended value at 298 K (Cantrell et al., 1993).
[c] Calculated from the ratio (k_2/k_{-2}) of the Atkinson's recommended values at 296 K.
[d] These rate constants are chamber dependent (on the size and the material of the chamber).

chemical reaction	constant	k (this work) at 296 K with k_2 fixed [a]	k (this work) at 296 K with k_{-2} fixed [a]	k (literature data) at 296 K
$NO_2 + O_3 \rightarrow NO_3 + O_2$	k_1 (cm^3 $molecule^{-1}$ s^{-1})	3.32×10^{-17}	3.31×10^{-17}	3.33×10^{-17} [a]
$NO_2 + NO_3 + M \leftrightarrow N_2O_5 + M$	k_2 (cm^3 $molecule^{-1}$ s^{-1})		1.19×10^{-12}	1.25×10^{-12} [a]
	k_{-2} (s^{-1})	3.62×10^{-2} s^{-1}		3.48×10^{-2} s^{-1} [a]
	K_{eq}			2.9×10^{-11} [b]
				3.59×10^{-11} [c]
$NO_3 \rightarrow$ wall losses	k_3 (s^{-1})	1.53×10^{-2} s^{-1} [d]	1.53×10^{-2} s^{-1} [d]	
$O_3 \rightarrow$ wall losses	k_4 (s^{-1})	7.54×10^{-5} s^{-1} [d]	7.53×10^{-5} s^{-1} [d]	

[a] Recommended value at 296 K, Atkinson et al., 2004 (IUPAC-web version, 2004).
[b] Recommended value at 298 K (Cantrell et al., 1993).
[c] Calculated from the ratio (k_2/k_{-2}) of the Atkinson's recommended values at 296 K.
[d] These rate constants are chamber dependent (on the size and the material of the chamber).

Summary

Contrary to long-lived species such as GHG, monitoring of strongly reactive short-lived species (concentration, flux, vertical profile) **represent a real challenge** in terms of sensitivity, accuracy, precision, time response, interference from sampling / analytical artifacts, calibration, ….

Very low-cost UV-VIS LED sources permits *multiple species quantification with high sensitivity*

Mid-IR LASER offers the unique advantage of *real time spectroscopic analysis of the isotopic composition* of the key atmospheric species, which is crucial for study of the *origin*, *evolution* and *dispersion* of these chemical species in the atmosphere for well understanding tropospheric process.

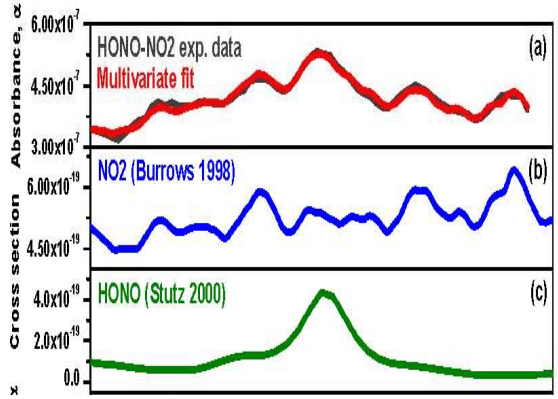

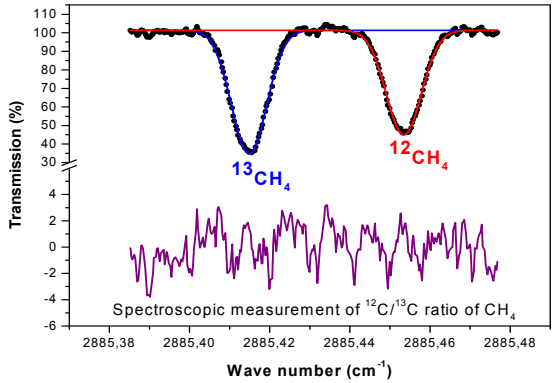

Collaborators

W. Zhao, T. Wu, X. Cui, C. Lengignon, R. Maamary, E. Fertein, C. Coeur, A. Cassez Université du Littoral Côte d'Opale, France

G. Wysocki Electrical Engineering Department, Princeton University, USA

G. Zha, Zheng Xu, T. Wang Department of Civil and Structural Engineering, The Hong Kong Polytechnic University, China

Y. Wang, W. Zhang, X. Gao, W. Liu, F. Dong Anhui Institute of Optics & Fine Mechanics, Hefei, China

The IRENI program of the Région Nord-Pas de Calais.

The Program of the Groupement de Recherche International SAMIA between CNRS (France), RFBR (Russia) and CAS (China)

The FR-ANR & US-NSF International Program

Thank You

Questions & Comments ....

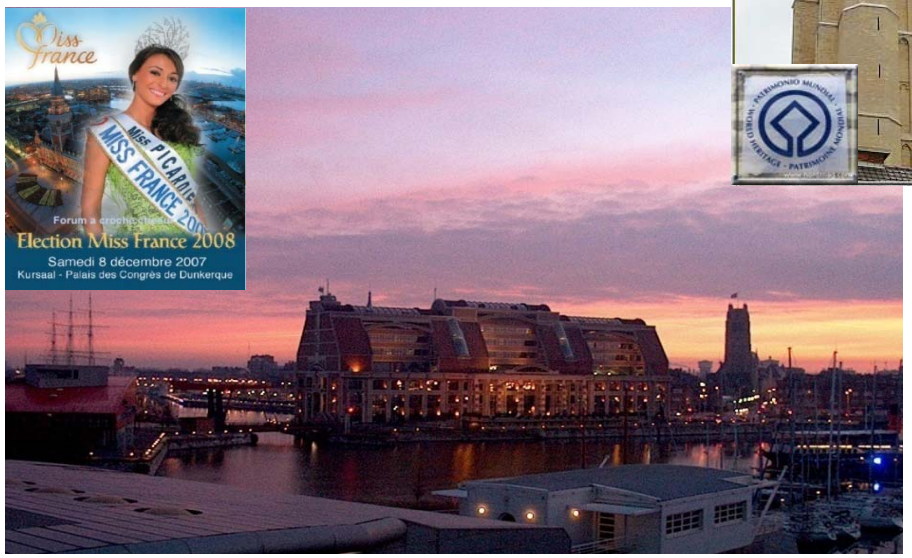

MIOMD 2014

Infrared Optoelectronics : Materials and Devices

October 5-8, 2014, Montpellier, FRANCE

Infrared Emission and Detection:

Interband and inter-subband physics/modeling, material growth and characterization, and device processing. Novel architectures. Non-linear technologies. Radiation effects. Systems components.

Infrared Integrated Systems:

Monolithic and heterogeneous integration of lasers, detectors, and passive components.

Scene illumination, standoff chemical-specific imaging, environmental monitoring, LIDAR, free-space communication.

Infrared Applications of Infrared Emission / Detection:

Applications of infrared detectors and lasers.

New in MIOMD 2014: larger "Sensing session"